The interaction of vorticity and rate-of-strain in homogeneous sheared turbulence

K. K. Nomura[a] and P. J. Diamessis
Department of Mechanical and Aerospace Engineering, University of California at San Diego, La Jolla, California 92093-0411

(Received 19 August 1998; accepted 20 December 1999)

The coupled interaction of vorticity ω and rate-of-strain S in homogeneous sheared turbulence is investigated using direct numerical simulation. Conditional sampling and comparison with linear simulations reveal various aspects of the structure and dynamics. Due to the influence of the imposed ω and S, distinct directional features develop. Initial stretching of fluctuating ω by mean extensional strain and the presence of mean vorticity establish a *predominant* misalignment of ω with respect to the principal axes of S. The associated locally induced rotation of the S axes results in preferred orientations in ω and S. In high amplitude rotation-dominated regions of the flow, distinct characteristics are exhibited by the pressure Hessian Π due to the presence of small-scale spatial structure. Nonlocally induced S axes rotation through Π tends to counteract locally induced rotation in these regions. These features are absent in the linear flow which suggests a lack of spatial coherence in the corresponding intense ω^2 regions. High amplitude strain-dominated and comparable rotation-strain regions are also considered. In general, the high amplitude conditional samples capture the main features of the flow. The underlying behavior of ω and S is essentially the same as in isotropic turbulence; the directional preferences observed in shear flow demonstrate the physical implications of the associated mechanisms. Although there is greater directional variation in flows with high $\mathrm{Re}_\lambda/\mathrm{Sh}$, results indicate the significance of the persistence of mean shear.
 [S1070-6631(00)01304-0]

I. INTRODUCTION

The interaction of the vorticity vector ω and the rate-of-strain tensor S through vortex stretching is considered a primary mechanism in the generation and associated dynamics of the small scales in three-dimensional incompressible turbulence. Knowledge of the behavior of ω and S is, therefore, fundamental for precise descriptions of the flow. As described by the evolution equation for ω

$$\frac{D\omega_i}{Dt} = S_{ik}\omega_k + \nu\frac{\partial^2\omega_i}{\partial x_k \partial x_k}, \tag{1.1}$$

vortex stretching, $S_{ik}\omega_k$, represents the response of ω to S. Implicit is the coupled, nonlocal nature of the interaction which is indicated by the evolution equation for S

$$\frac{DS_{ij}}{Dt} = -S_{ik}S_{kj} - \frac{1}{4}(\omega_i\omega_j - \delta_{ij}\omega_k\omega_k) - \frac{1}{\rho}\frac{\partial^2 p}{\partial x_i \partial x_j} + \nu\frac{\partial^2 S_{ij}}{\partial x_k \partial x_k}. \tag{1.2}$$

In addition to self-interaction, effects of local ω, and viscous diffusion, the evolution of S_{ij} involves local and nonlocal action through the pressure field as described by the Hessian, $\partial^2 p/\partial x_i \partial x_j$. From here on we will use Π_{ij} to denote $\partial^2 p/\partial x_i \partial x_j$ and normalize density such that $\rho = 1$.

Previous work by Nomura and Post[1] describes the coupled interaction of ω and S in the principal strain basis. Here, the principal eigenvalues of S are identified as $\alpha \geqslant \beta \geqslant \gamma$ with the corresponding eigenvectors $\mathbf{e}_\alpha$, $\mathbf{e}_\beta$, and $\mathbf{e}_\gamma$. In this reference frame, interaction through vortex stretching and through rotation of the principal axes of S are distinguished; the latter associated with the condition of misaligned ω with respect to the S axes. As demonstrated by restricted Euler[2] equations (see Sec. II), locally induced rotation of the S axes acts to orient ω towards the direction of either the intermediate ($\mathbf{e}_\beta$) or most compressive ($\mathbf{e}_\gamma$) principal strain. Results from direct numerical simulations (DNS) of homogeneous isotropic turbulence[1] show the significance of this mechanism in the dynamics of the flow, particularly in high amplitude rotation-dominated regions which are known to concentrate into tube-like or filamentary structures.[1,3,4] Nonlocally induced rotation of the S axes through the pressure Hessian Π is found to counteract the locally induced rotation. This tendency is associated with the proximate spatial structure of these regions which controls Π. In general, the study demonstrates that the observed preferential alignment of ω and $\mathbf{e}_\beta$ in homogeneous turbulence[5–7] is a consequence of the dynamics of the coupled ω and S system.

Distinct structures are also present in homogeneous sheared turbulence. Regions of relatively high magnitude ω form tube-like and sheet-like structures[8,9] as well as hairpin-shaped vortices.[10] Such structures are found to be particularly active sites for momentum and scalar transport.[11] Due

[a]Electronic mail: knomura@mae.ucsd.edu

to the presence of mean shear, these structures tend to possess preferential spatial orientation;[7,9,10] at least for the flow times and Reynolds numbers investigated. Longitudinal vortex tubes and the associated ω are found to orient upwards from the streamwise direction at angles of 20°–45°. This is due, in part, to stretching of ω by the extensional strain associated with the mean shear. The generated strain from these structures are presumed to enhance spanwise vorticity which may then form lateral vortex layers.[9] Preferential alignment of ω and $\mathbf{e}_\beta$ is also observed in these flows.[6,7] In general, however, these previous analyses have focused on ω and direct examination of S has not been carried out. Although basic features of the early development of inclined and hairpin-like structures have been described by considering rapid distortion theory (RDT),[9,12] the complex nonlinear interaction in the presence of mean shear is not fully understood.

In this paper, we consider the structure and dynamics associated with the coupled interaction of ω and S in homogeneous sheared turbulence. Results from DNS are investigated. In particular, we present characteristics of S and Π, which previously have not been considered, in order to provide a more complete description of this flow. Results demonstrate the dynamics described in the principal strain basis and further, depict the physical implications of the associated mechanisms. The development of the observed directional features is explained in terms of the influence of the imposed ω and S on these mechanisms. This illustrates the effects of mean flow on small-scale motion. Such understanding of ω and S is requisite for the analysis of more complex flows, e.g., shear flows with stratification and buoyancy. With shear and stratification, directional features in ω and S affect the behavior of the scalar (density) gradient, $\mathbf{G}$. When buoyancy effects are present, $\mathbf{G}$ will feedback on the flow and the associated dynamics constitute a complex triadic interaction between ω, S, and $\mathbf{G}$.[13]

We begin with a brief summary of the analysis framework. This is followed by presentation of the DNS results.

II. DYNAMICS OF ω AND S

In the analysis of the coupled dynamics of ω and S, it is advantageous to express Eqs. (1.1) and (1.2) in the principal strain basis[1]

$$\begin{aligned}
\frac{D\omega_\alpha}{Dt} &= \alpha\omega_\alpha + \nu\nabla^2\omega_\alpha + \omega_\beta\dot{\Omega}_{\mathbf{e}_\alpha-\mathbf{e}_\beta} + \omega_\gamma\dot{\Omega}_{\mathbf{e}_\alpha-\mathbf{e}_\gamma},\\
\frac{D\omega_\beta}{Dt} &= \beta\omega_\beta + \nu\nabla^2\omega_\beta + \omega_\alpha\dot{\Omega}_{\mathbf{e}_\beta-\mathbf{e}_\alpha} + \omega_\gamma\dot{\Omega}_{\mathbf{e}_\beta-\mathbf{e}_\gamma},\\
\frac{D\omega_\gamma}{Dt} &= \gamma\omega_\gamma + \nu\nabla^2\omega_\gamma + \omega_\alpha\dot{\Omega}_{\mathbf{e}_\gamma-\mathbf{e}_\alpha} + \omega_\beta\dot{\Omega}_{\mathbf{e}_\gamma-\mathbf{e}_\beta},\\
\frac{D\alpha}{Dt} &= -\alpha^2 + \frac{1}{4}(\omega_\beta^2+\omega_\gamma^2) - \tilde{\Pi}_{\alpha\alpha} + \nu\nabla^2\alpha,\\
\frac{D\beta}{Dt} &= -\beta^2 + \frac{1}{4}(\omega_\alpha^2+\omega_\gamma^2) - \tilde{\Pi}_{\beta\beta} + \nu\nabla^2\beta,
\end{aligned} \tag{2.1}$$

$$\frac{D\gamma}{Dt} = -\gamma^2 + \frac{1}{4}(\omega_\alpha^2+\omega_\beta^2) - \tilde{\Pi}_{\gamma\gamma} + \nu\nabla^2\gamma, \tag{2.2}$$

where $\tilde{\Pi}$ denotes the pressure Hessian in this basis. The first three equations [Eq. (2.1)] describe the evolution of ω in which vortex stretching is clearly distinguished and the next three equations [Eq. (2.2)] govern the total rate of change of the principal eigenvalues. In Eq. (2.1), the third and fourth terms on the right-hand-side represent changes in the ω components due to $\dot{\Omega}$ which gives the effective rate of rotation of the principal axes,[1] e.g.,

$$\begin{aligned}
\dot{\Omega}_{\mathbf{e}_\alpha-\mathbf{e}_\beta} &\equiv \frac{D\mathbf{e}_\alpha}{Dt}\cdot\mathbf{e}_\beta - \nu(\nabla^2\mathbf{e}_\alpha)\cdot\mathbf{e}_\beta\\
&= -\frac{1}{\alpha-\beta}\left(\frac{1}{4}\omega_\alpha\omega_\beta + \tilde{\Pi}_{\alpha,\beta}\right).
\end{aligned} \tag{2.3}$$

Specifically, $\dot{\Omega}_{\mathbf{e}_\alpha-\mathbf{e}_\beta}$ represents the rate of rotation in the plane comprised of $\mathbf{e}_\beta$ and $\mathbf{e}_\alpha$ about an axis coinciding with $\mathbf{e}_\gamma$. The right-hand-side of Eq. (2.3) indicates that a rotation of the principal axes may be induced by both local ($\omega_\alpha\omega_\beta$) and nonlocal ($\tilde{\Pi}_{\alpha,\beta}$) effects (designation of these effects as local and nonlocal is explained below).

By applying the assumptions of the restricted Euler problem[2,14] which consider Π to be isotropic, Eq. (2.1) becomes[1]

$$\begin{aligned}
\frac{D\omega_\alpha}{Dt} &= \alpha\omega_\alpha - \frac{1}{4}\frac{\omega_\beta\omega_\alpha}{\alpha-\beta}\omega_\beta - \frac{1}{4}\frac{\omega_\gamma\omega_\alpha}{\alpha-\gamma}\omega_\gamma,\\
\frac{D\omega_\beta}{Dt} &= \beta\omega_\beta + \frac{1}{4}\frac{\omega_\alpha\omega_\beta}{\alpha-\beta}\omega_\alpha - \frac{1}{4}\frac{\omega_\gamma\omega_\beta}{\beta-\gamma}\omega_\gamma,\\
\frac{D\omega_\gamma}{Dt} &= \gamma\omega_\gamma + \frac{1}{4}\frac{\omega_\alpha\omega_\gamma}{\alpha-\gamma}\omega_\alpha + \frac{1}{4}\frac{\omega_\beta\omega_\gamma}{\beta-\gamma}\omega_\beta.
\end{aligned} \tag{2.4}$$

The second and third terms on the right-hand-side of Eq. (2.4) are arranged so that the quantities in the denominator, e.g., $(\alpha-\beta)$, are always positive (based on the defined α,β,γ), and thus the signs preceding these terms indicate the resulting effect for each vorticity component. This shows that local ω, if misaligned with the principal axes, rotates the principal axes in such a way to orient ω *away from* the $\mathbf{e}_\alpha$ direction and *towards* that of either $\mathbf{e}_\beta$ or $\mathbf{e}_\gamma$. Solutions to the restricted Euler equations show that, for initially misaligned ω, the limiting configuration in the presence of strain generation, locally induced strain axes rotation, and vortex stretching–contraction is the alignment of ω with $\mathbf{e}_\beta$. Since Π is assumed isotropic, the equations are autonomous and effectively describe the local dynamics of a fluid particle.[2] The anisotropic component of Π, which contributes to the S axes rotation, then represents deviation from the restricted Euler problem and, in this sense, is regarded as nonlocal. In fully developed turbulence, although a preference for alignment of ω and $\mathbf{e}_\beta$ is exhibited, overall, misalignment of ω prevails. The propensity for ω to orient towards $\mathbf{e}_\beta$ in turbulent flows suggests that this is the state in which events have the longest duration.

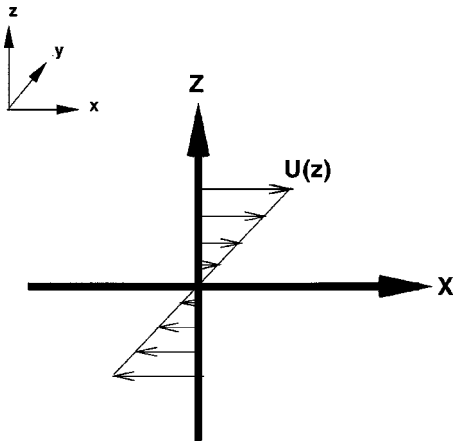

FIG. 1. Sketch of mean velocity profile and coordinate system.

The previous study[1] demonstrated these dynamics in isotropic turbulence. We now consider the case of homogeneous shear flow in which an imposed mean ω and S are present.

III. DIRECT NUMERICAL SIMULATIONS

A. Simulation description

The nondimensional parameters describing homogeneous sheared turbulence are the turbulent Reynolds number based on the Taylor microscale

$$\mathrm{Re}_\lambda = \frac{v\lambda}{\nu} = \frac{v^2/\varepsilon}{1/\langle\omega'\rangle}, \tag{3.1}$$

which effectively gives the ratio of the time scale associated with the large-scale turbulent motion to that of the small-scale, and the Shear number

$$\mathrm{Sh} = \frac{v^2/\varepsilon}{1/S} \tag{3.2}$$

which is the ratio of the time scale of the large-scale turbulence to that of the mean flow. Then

$$r_\omega = \frac{\mathrm{Re}_\lambda}{\mathrm{Sh}} = \frac{\langle\omega'\rangle}{S}, \tag{3.3}$$

indicates the relative strength of fluctuating vorticity to mean vorticity. In the above expressions, v is the rms velocity, ε is the energy dissipation rate, ν is the kinematic viscosity, and S is the mean shear.

Two sets of DNS of homogeneous shear flow results are considered in the analysis. These provide a range of Sh and Re_λ values thereby giving a range of r_ω. The governing equations describing the incompressible flow are the three-dimensional, time-dependent continuity and Navier–Stokes equations. Figure 1 shows the uniform mean velocity profile $U(z)$ corresponding to the mean shear and the coordinate system used.

The first set are the results of DNS of homogeneous sheared turbulence that we have performed in order to obtain complete information on the flows. In these simulations, the computational domain is a finite cube with sides of length L, containing 128^3 grid points. The reference value for velocity is $\Delta U = (dU/dz)_{\mathrm{ref}} L$. The nondimensional shear S is defined as $S = (L/\Delta U)(dU/dz)_{\mathrm{ref}} = 1$. Periodic boundary conditions are employed in the x (streamwise) and y (spanwise) directions and shear-periodic conditions[15] in the z (mean velocity gradient) direction. The simulations are initialized with a fully developed isotropic velocity field obtained from simulations of unforced isotropic turbulence. The numerical solution employs a pseudospectral method. Details of the computational procedures are given elsewhere.[7,15] Simulations have been performed for various parameter values. Here, we present results for two cases, parameterized by their initial values. In the first case, $\mathrm{Re}_{\lambda_0} = 24$, $\mathrm{Sh}_0 = 1.5$; thus $r_{\omega_0} = 16$. We will refer to this simulation as RLOW1. In the second case, $\mathrm{Re}_{\lambda_0} = 29$, $\mathrm{Sh}_0 = 16.0$; thus $r_{\omega_0} = 1.8$. We will refer to this simulation as RLOW2. The two flows have comparable Re_{λ_0} but differ significantly in r_{ω_0}.

The second set of DNS used in the analysis are those of Jacobitz *et al.*[16,17] These spectral simulations of homogeneous shear flow provide single time data sets at additional Sh and Re_λ values. In the results presented here, $\mathrm{Re}_{\lambda_0} = 44.7$ and $\mathrm{Sh}_0 = 2.0$. Thus, $r_{\omega_0} = 22.4$. Since the Re_{λ_0} is higher than the RLOW flows, we designate this simulation as RHIGH. The database provides full flow field data at two different nondimensional times, $\mathrm{St} = 3$ and $\mathrm{St} = 9$, representing relatively early and later times in the development of the flow. These simulations are also initialized with fully developed isotropic turbulence. Complete details are given elsewhere.[16]

The overall behavior of the RLOW and RHIGH flows are similar; after a short period of decay due to the initial isotropic conditions,[17] the turbulent kinetic energy increases in time for the duration of the simulations. In this study, we focus our attention on small-scale (derivative) quantities. From the computed flow field, various quantities associated with the velocity gradient tensor (ω and S) and pressure Hessian Π are evaluated. From S, the three principal eigenvalues ($\alpha \geqslant \beta \geqslant \gamma$) and corresponding eigenvectors ($\mathbf{e}_\alpha$, $\mathbf{e}_\beta$, $\mathbf{e}_\gamma$) are evaluated. Similarly, Π is evaluated and the principal eigenvalues ($\phi_1 \geqslant \phi_2 \geqslant \phi_3$) are determined along with their corresponding eigenvectors, $\mathbf{f_1}$, $\mathbf{f_2}$, $\mathbf{f_3}$. Ensemble (spatial) averaged quantities will be denoted by brackets $\langle\rangle$. Time is nondimensionalized by S.

B. Conditional sampling

In the results to be presented, conditional statistics associated with distinct high amplitude events are considered. Recall that the *local* flow can be characterized in terms of the invariants of the velocity gradient tensor. For an incompressible flow, the three invariants may be expressed as[1]

$$I = -(\alpha+\beta+\gamma) = 0, \tag{3.4}$$

$$II = \tfrac{1}{2}(\omega^2/2 - \mathsf{S}^2), \tag{3.5}$$

$$III = -\alpha\beta\gamma - \tfrac{1}{4}(\alpha\omega_\alpha^2 + \beta\omega_\beta^2 + \gamma\omega_\gamma^2). \tag{3.6}$$

Local flow conditions may therefore be represented by a point in the $II-III$ plane. Figure 2 shows joint probability

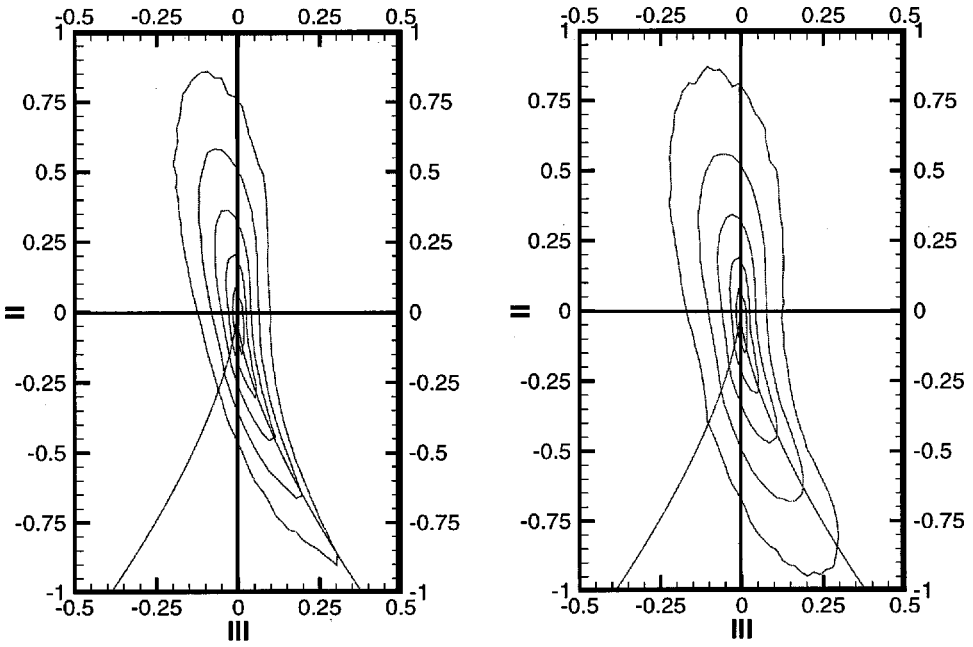

FIG. 2. Joint probability distribution of the tensor invariants II and III (normalized by $\langle\omega^2\rangle$ and $\langle\omega^2\rangle^{3/2}$, respectively) for (a) RLOW1: $r_{\omega_0}=16$, St=6, (b) RHIGH: $r_{\omega_0}=22.4$, St=9. Contour values correspond to $\log(10^6 P+1)$ where P is the probability. The minimum and maximum contour levels are 2.0 and 4.5, respectively, where the latter corresponds to the inner most contour.

distributions in the $II-III$ plane for the RLOW1 and RHIGH flow fields. The values of II and III are normalized by $\langle\omega^2\rangle$ and $\langle\omega^2\rangle^{3/2}$, respectively, for the given time. The zero discriminant curve which separates complex and real eigenvalues is included in these plots. The distributions of both flows are generally similar showing highest probability occurring near the origin and distinct preferences for the upper left and lower right quadrants as is observed in various turbulent flows.[18] As discussed by Nomura and Post,[1] pathlines for a Burgers vortex tube appear as straight lines extending from the lower right to upper left quadrant in the $II-III$ plane; the observed features, therefore, suggest the presence of stretched vortices.

Based on the observed $II-III$ preferences, we select three conditional samples for this study and these are referred to by the particular quadrant or region of the $II-III$ plane that they represent. By definition of II (3.5), the QII ($II>0$, $III<0$) sample is comprised of rotation-dominated events while the QIV ($II<0$, $III>0$) sample is comprised of strain-dominated events. These samples are restricted to events relatively far from the origin in the $II-III$ plane, $\sqrt{II^2+III^2}\geqslant r_{\text{th}}$ (where II and III are the normalized values). We also consider a sample Q0 comprised of regions of comparable and high levels of $\omega^2/2$ and S^2 ($II\sim 0$, $\omega^2 \geqslant r_{\text{th}}\langle\omega^2\rangle$). Thus, Q0 represents high amplitude events at the origin of the $II-III$ plane. In each sample, the threshold level r_{th} is adjusted so that the sample size is $\sim$5% of the total grid points.

In general, we expect that these high-amplitude events will more clearly display and emphasize the associated characteristic behavior for the sampled region. As will be discussed in the next section, isosurfaces identified by II exhibit fundamentally distinct spatial structure. Implications of III on structure have also been demonstrated.[1] Conditional sampling based on the invariants will therefore extract characteristics and behavior associated with particular structure. Consideration of II will also assist in distinguishing various mechanisms by considering the relative significance of rotation versus strain.

C. Structure of ω and S

In this section, we present structural characteristics of the RHIGH ($r_{\omega_0}=22.4$) flow in which $\langle\omega'\rangle$ is significant. As discussed in the Introduction, distinct spatial structures are present in homogeneous sheared turbulence. Here, we consider the spatial structure of regions characterized by II. Figure 3 shows three-dimensional visualizations of isoscalar surfaces of high positive values of II. The figure displays both top and side views of the flow at St=3 [Figs. 3(a) and 3(b)] and St=9 [Figs. 3(c) and 3(d)]. As shown in Nomura and Post,[1] high amplitude $II>0$ regions in isotropic turbulence exhibit tube-like spatial structure. In this flow, however, the structures exhibit distinct spatial orientation. From the side views [Figs. 3(b) and 3(d)], we see that the tubes orient at $\sim$20°–45° from the streamwise direction with slightly smaller angles at the later time. The top views show that early in time [Fig. 3(a)], the tubes generally orient along the streamwise direction while later [Fig. 3(c)], the tubes incline towards the spanwise direction. We have also visualized high amplitude strain-dominated ($II<0$) and Q0 ($II\sim 0$) regions (not shown). The $II<0$ regions do not coincide with rotation-dominated structures although they tend to occur in their vicinity. In general, these regions are not as geometrically distinct as those of $II>0$; the corresponding isoscalar surfaces are irregular and tend to be more discontinuous with limited spatial extent. The Q0 regions (comparable rotation and strain) tend to form sheet-like

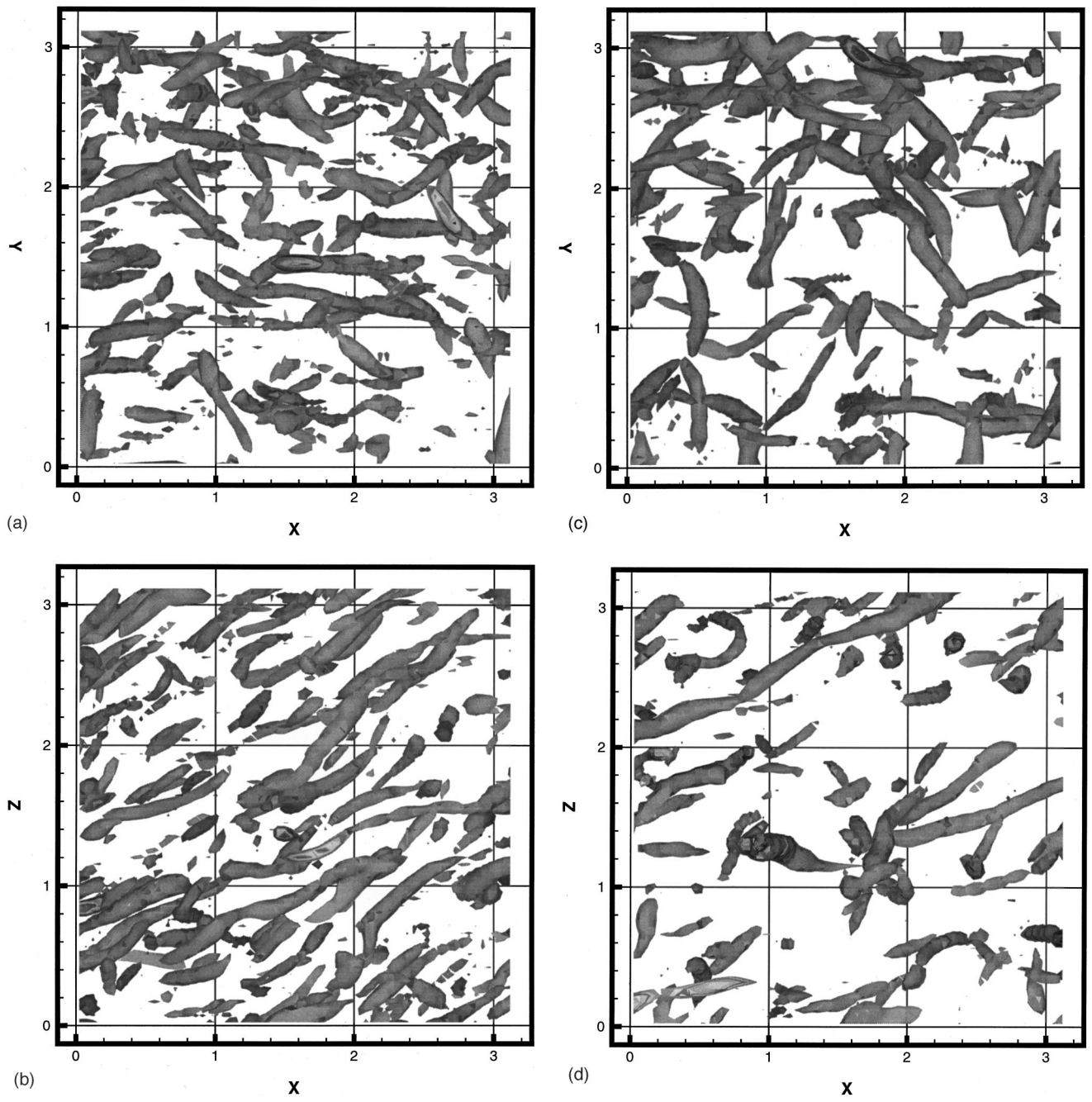

FIG. 3. Three-dimensional visualizations (64^3 subdomain of computational box) of high amplitude rotation dominated ($II>0$) regions in homogeneous shear flow (RHIGH); (a) top view, St=3, (b) side view, St=3, (c) top view, St=9, (d) side view, St=9. Isoscalar surfaces represent same threshold magnitude of II ($0.6\langle\omega^2\rangle$) in all cases.

structures with significant spatial extent in the streamwise and spanwise directions. These structures tend to tilt from the horizontal in the spanwise direction.

In order to investigate the flow structure in detail, we examine the spatial orientation of ω and the eigenvectors of S. The orientation of any vector $\mathbf{v}$ in the coordinate space can be defined by the angle pair $(\theta_{\text{pitch}}, \theta_{\text{yaw}})$ where θ_{pitch} is the angle of the vector from its projection in the $x-y$ (horizontal) plane and θ_{yaw} is the angle of the projection in the $x-y$ plane from the positive y axis (see Fig. 4). Since (0°, 0°) is the orientation of the vorticity $\overline{\omega}$ associated with the mean shear, the angle pair gives the orientation of a vector with respect to this reference direction. Joint probability distributions (JPD) for $(\theta_{\text{pitch}}, \theta_{\text{yaw}})$ should then indicate the most probable orientation for a given sample. With the geometry as defined, however, it can be shown that the probability density function of a random vector to orient at a particular θ_{pitch} is $\frac{1}{2}\cos\theta_{\text{pitch}}$, i.e., there is inherently a greater probability for $\theta_{\text{pitch}}=0°$ than for $\theta_{\text{pitch}}=90°$. To eliminate this bias, the quantity $\sin\theta_{\text{pitch}}$ rather than θ_{pitch} is used to generate the angle pair JPD plots which effectively indicate the probable $(\theta_{\text{pitch}}, \theta_{\text{yaw}})$.

The orientation of instantaneous ω in the total flow field (not shown) is in agreement with previous studies.[7,9,10] The

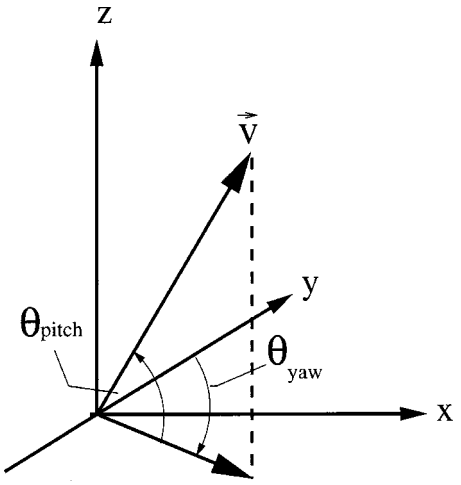

FIG. 4. Definition of the angles of orientation ($\theta_{\text{pitch}}, \theta_{\text{yaw}}$) of a vector in 3D (three-dimensional) cartesian coordinates.

distribution at early time (St=3) displays peaks corresponding to ($\theta_{\text{pitch}}, \theta_{\text{yaw}}$)=($\pm 35°, \pm 60°$). At a later time (St=9), the distribution remains nearly the same although θ_{yaw} tends to increase by ~5°–10°. Distributions for ω in the QII and Q0 conditional samples are shown in Fig. 5. In the QII sample [Figs. 5(a) and 5(b)], at the early time, a preference of ω to orient at ~($\pm 30°$, $\pm 80°$) is indicated while at the later time, θ_{yaw} exhibits a greater range of values $\pm 30°$ about $|\theta_{\text{yaw}}| = 90°$. This is generally consistent with the orientation of the structures in Fig. 3. In Q0 [Figs. 5(c) and 5(d)], the spanwise component becomes progressively more significant in time. At St=9, a dominant positive spanwise component and a range of θ_{pitch} is exhibited. The distributions for QIV (not shown) at both early and later times resemble those of Q0 at St=9. In general, the combined results of QII and Q0 regions capture the dominant features of ω in the total flow.

Figure 6 shows ($\theta_{\text{pitch}}, \theta_{\text{yaw}}$) for the fluctuating vorticity $\omega' = \omega - \overline{\omega}$ for the QII and Q0 samples at St=9. Note that in both samples, the peaks in ω' occur at $|\theta_{\text{yaw}}| > 90°$ as compared with $|\theta_{\text{yaw}}| \leqslant 90°$ for ω (Fig. 5). In QII, there is a tendency towards smaller $|\theta_{\text{pitch}}|$ which develops in time. In the strain-dominated QIV regions (not shown), there is generally greater variation in the direction of ω'. At early time, the peaks are similar to those in Q0 and exhibit $|\theta_{\text{yaw}}|$

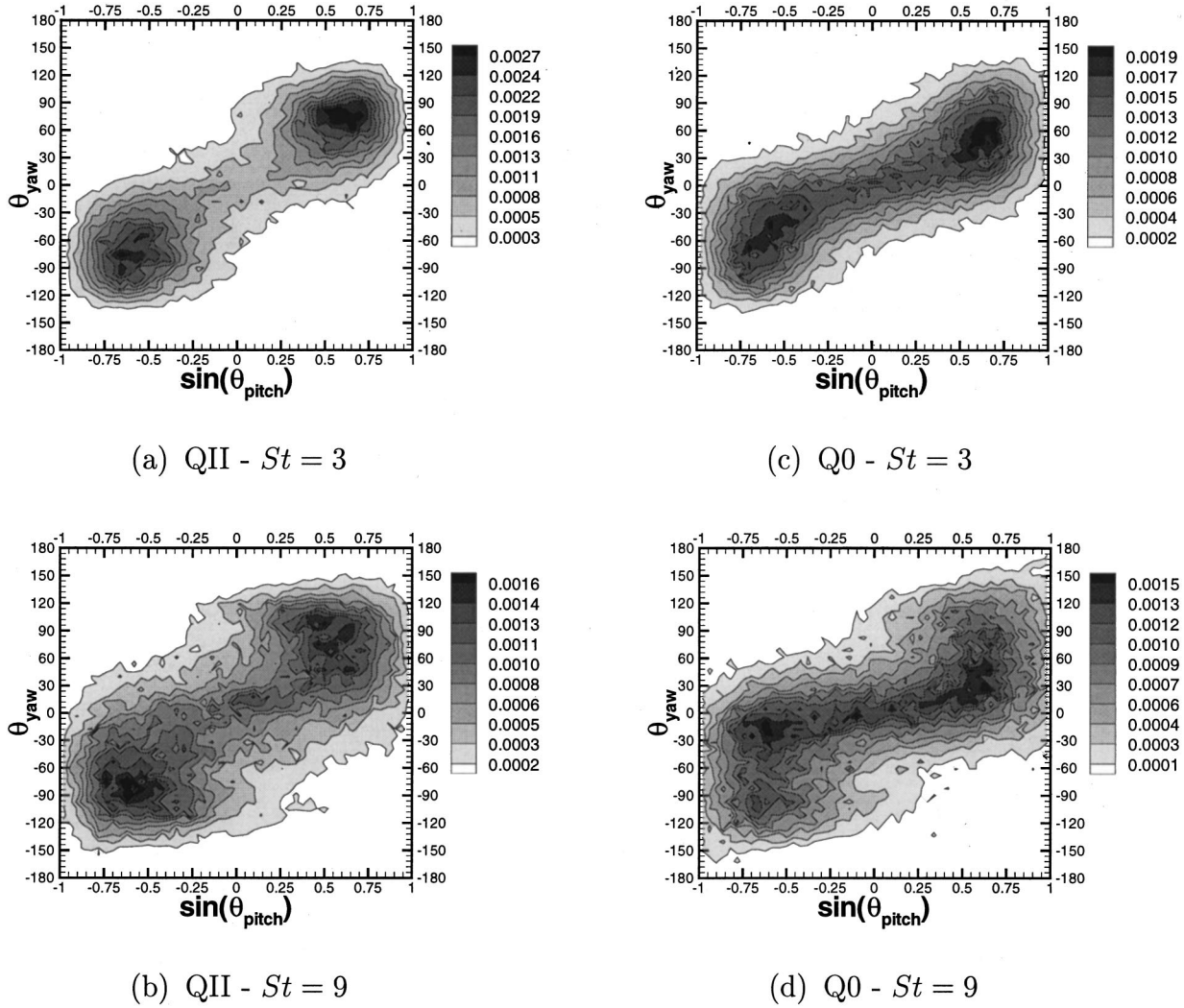

(a) QII - $St = 3$ (c) Q0 - $St = 3$

(b) QII - $St = 9$ (d) Q0 - $St = 9$

FIG. 5. Joint probability distributions indicating the angles of orientation ($\theta_{\text{pitch}}, \theta_{\text{yaw}}$) of ω for RHIGH: (a) QII, St=3, (b) QII, St=9, (c) Q0, St=3, (d) Q0, St=9 (sample thresholds are QII: $r_{\text{th}} = 0.40$ and Q0: $r_{\text{th}} = 1.3$).

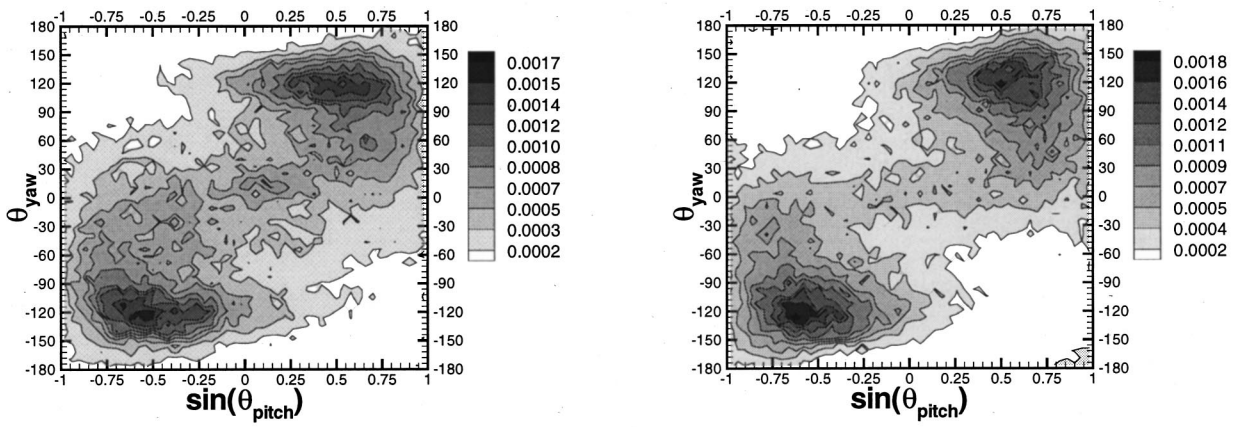

(a) QII (b) Q0

FIG. 6. Joint probability distributions indicating the angles of orientation ($\theta_{\text{pitch}}, \theta_{\text{yaw}}$) of ω' for RHIGH (St=9): (a) QII, (b) Q0.

$>90°$ while later in time, a preference for $\theta_{\text{yaw}}=0°$ develops. In all samples, the probability curves for both ω and ω' tend to follow a reverse ''S'' shape. As noted by Rogers and Moin,[10] this shape resembles the curve representing a plane aligned with the y axis and inclined upwards from the horizontal at 45° from the positive x axis [see Figs. 9(a) and 9(c)]. We will refer to this plane as the ''S^+-plane'' of which the significance will later be explained.

We now consider the orientation of the principal axes of S. Recall that the lines of action of $\overline{\mathbf{e}}_\alpha$, $\overline{\mathbf{e}}_\beta$, and $\overline{\mathbf{e}}_\gamma$ associated with the mean shear are $(\pm 45°, \pm 90°)$, $(0°, 0°)$, and $(\pm 45°, \mp 90°)$, respectively. Here, we consider the (positive) direction of the eigenvectors as designated by the local vorticity.[1] Figures 7(a)–7(c) gives the angle pair JPDs for the total flow at St=9. The distributions at the earlier time (not shown) are generally similar; the peaks occur at nearly the same locations although the distributions show less variation. This suggests that some condition of equilibrium is established. In the JPD for $\mathbf{e}_\alpha$, the shape of the distribution generally follows the S^+-plane curve. Note that the peaks occur at $|\theta_{\text{yaw}}|>90°$. In the JPD for $\mathbf{e}_\gamma$ [Fig. 7(c)], the distributions follow a *forward* ''S''-shape suggesting that $\mathbf{e}_\gamma$ lies nearly in the plane orthogonal to the S^+-plane, i.e., the S^--plane which is inclined from the horizontal at $-45°$ from the positive x axis. The corresponding peaks in $\mathbf{e}_\gamma$ occur at $|\theta_{\text{yaw}}| < 90°$. The orientation of $\mathbf{e}_\beta$ must of course be mutually orthogonal to $\mathbf{e}_\alpha$ and $\mathbf{e}_\gamma$. The distribution in Fig. 7(b) suggests that $\mathbf{e}_\beta$ tends to lie nearly in the S^+-plane although the curves also extend outward somewhat towards the direction of $\overline{\mathbf{e}}_\gamma$.

The orientation of the eigenvectors in the conditional samples are also examined. In the QII sample at early time (St=3, not shown), $\mathbf{e}_\alpha$ exhibits $|\theta_{\text{yaw}}|>90°$ while $\mathbf{e}_\beta$ exhibits a range $0°<|\theta_{\text{yaw}}|<90°$. At later time [St=9, Figs. 7(d)–7(f)], the distributions of $\mathbf{e}_\alpha$ and $\mathbf{e}_\beta$ become less distinct while the S^--plane curve shape is maintained in $\mathbf{e}_\gamma$. In the case of Q0 [Figs. 8(a) and 8(b)], the S^+-plane curve in $\mathbf{e}_\alpha$ is more apparent although the peaks indicate that $\mathbf{e}_\alpha$ tends to orient nearly in the direction of $\overline{\mathbf{e}}_\alpha$. In QIV [Figs. 8(c) and 8(d)], $\mathbf{e}_\alpha$ tends to orient in the spanwise direction while $\mathbf{e}_\beta$ orients near $\overline{\mathbf{e}}_\alpha$. The orientation of $\mathbf{e}_\gamma$ in Q0 and QIV (not shown) is similar to that in the total flow [Fig. 7(c)]. Note that the peaks in the total flow JPDs [Figs. 7(a) and 7(b)] do not necessarily correspond with those of the strain-dominated QIV sample [Figs. 8(c) and 8(d)]. In particular, the peak in the $\mathbf{e}_\alpha$ distribution for QIV [Fig. 8(c)] corresponds to the secondary peak in the corresponding distribution of the total flow [Fig. 7(a)]. Thus, in regards to directional features in S, Q0 and QIV regions together generally capture the dominant features observed in the total flow.

D. Dynamics of ω and S

We now consider the dynamics associated with the observed directional features. As discussed, the coupled dynamics of ω and S are effectively described in the principal strain basis (2.1) and (2.2). In addition to direct interaction through vortex stretching, ω and S interact through locally- and nonlocally induced rotation of the principal axes and generation of strain. We first consider the interaction of ω and S under conditions in which locally, the imposed mean flow dominates, i.e., the principal strain axes essentially coincide with those of the mean flow [Fig. 9(a)] and the mean vorticity $\overline{\omega}=S$ is effectively ω_β. Amplification due to vortex stretching in the initially isotropic field will be greatest (and persist) for the fluctuating component ω' in the direction of the largest extensional strain, $\overline{\mathbf{e}}_\alpha$. The *resultant* ω will then lie in the plane containing $\overline{\mathbf{e}}_\beta$ $(\overline{\omega})$ and $\overline{\mathbf{e}}_\alpha$, i.e., the S^+-plane. A *predominant misalignment* of ω with respect to the principal axes is thereby established which induces a rotation of the axes. This is illustrated in Fig. 9(b) which shows the S^+-plane and associated quantities. The corresponding rate of rotation is given by Eq. (2.3),

$$\dot{\Omega}_{\mathbf{e}_\alpha-\mathbf{e}_\beta}=-\frac{1}{\alpha-\beta}\left(\underbrace{\frac{1}{4}\omega_\alpha\omega_\beta}+\Pi_{\alpha,\beta}\right). \tag{3.7}$$

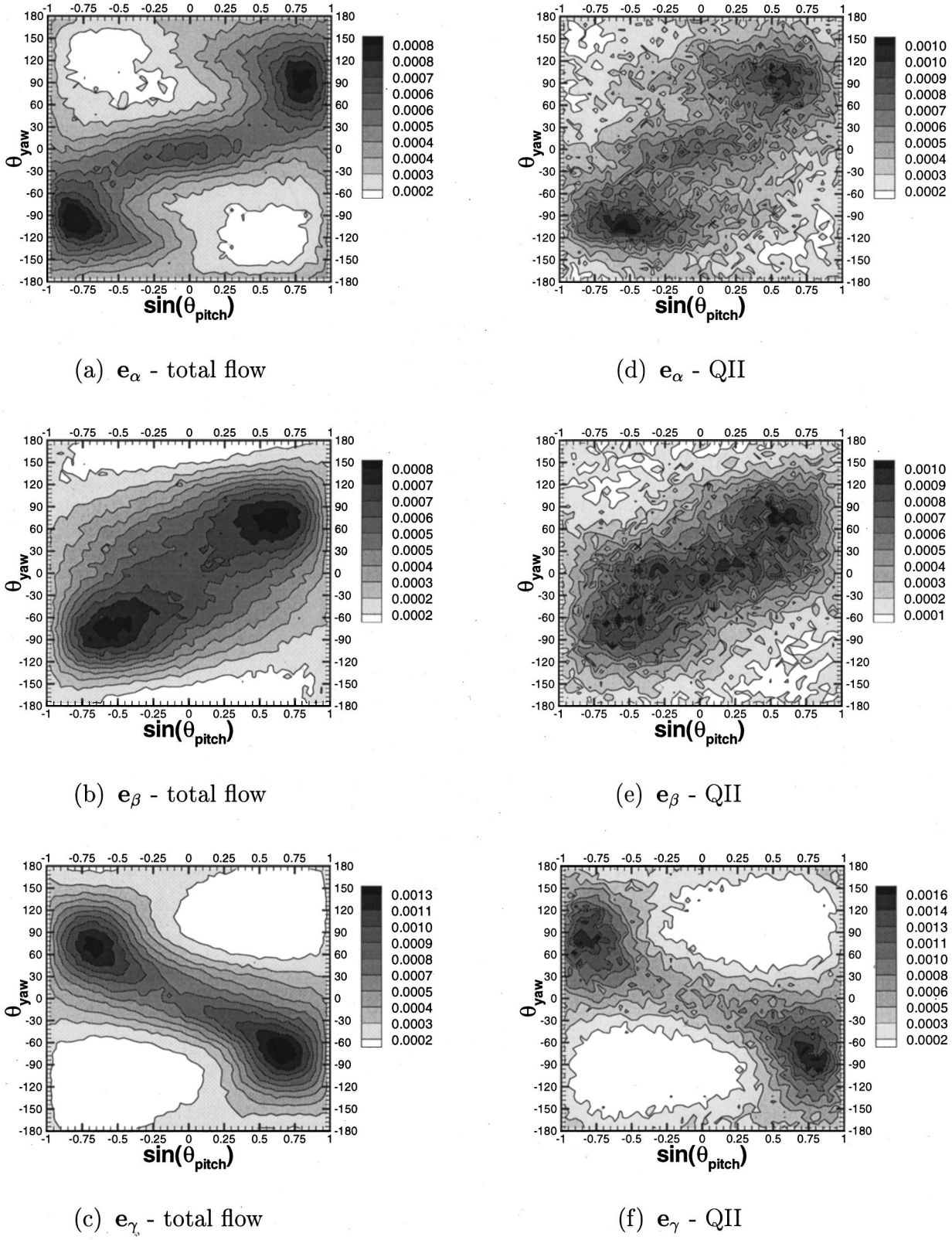

FIG. 7. Joint probability distributions indicating the angles of orientation ($\theta_{\text{pitch}}, \theta_{\text{yaw}}$) of eigenvectors for RHIGH at St=9; total flow: (a) $\mathbf{e}_\alpha$, (b) $\mathbf{e}_\beta$, (c) $\mathbf{e}_\gamma$, and QII conditioned sample: (d) $\mathbf{e}_\alpha$, (e) $\mathbf{e}_\beta$, (f) $\mathbf{e}_\gamma$.

Thus, if the eigenvectors initially coincide with $\overline{\mathbf{e}}_\alpha$ and $\overline{\mathbf{e}}_\beta$, locally induced rotation by misaligned ω, i.e., $\omega_\alpha \omega_\beta$, will reorient $\mathbf{e}_\alpha$ and $\mathbf{e}_\beta$ in the S^+-plane. As indicated by the restricted Euler equations [Eq. (2.4)], the sense of rotation is such that $\mathbf{e}_\alpha$ is directed *away* from ω. For the assumed conditions, this would result in $|\theta_{\text{yaw}}| > 90°$ for $\mathbf{e}_\alpha$. Further amplification of ω_α will occur along the altered principal strain axes [dashed lines in Fig. 9(b)]. If these local effects are

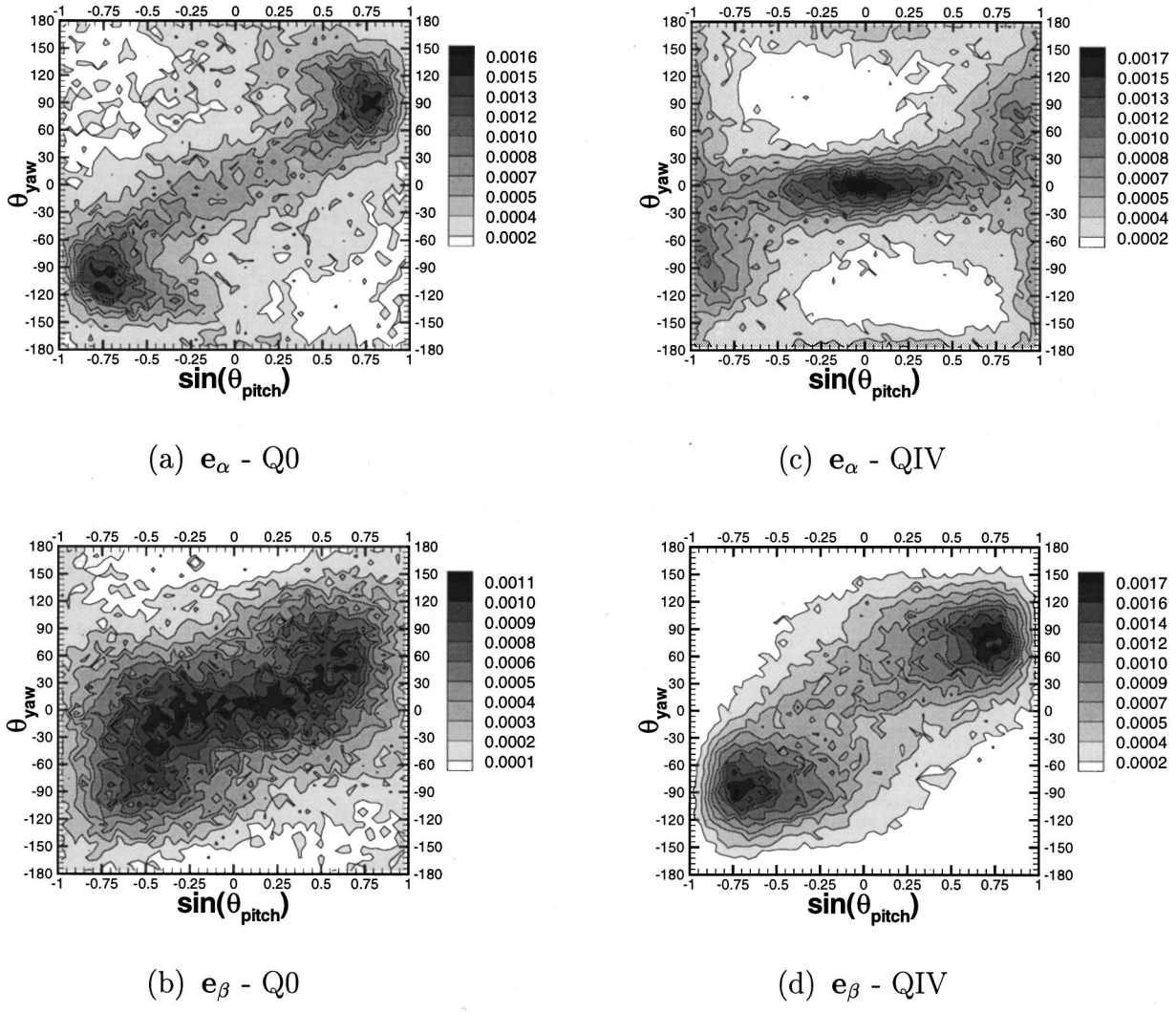

FIG. 8. Joint probability distributions indicating the angles of orientation ($\theta_{\text{pitch}}, \theta_{\text{yaw}}$) of $\mathbf{e}_\alpha$ and $\mathbf{e}_\beta$ eigenvectors for Q0 and QIV samples at St=9 (RHIGH): (a) $\mathbf{e}_\alpha$, Q0, (b) $\mathbf{e}_\beta$, Q0, (c) $\mathbf{e}_\alpha$, QIV, (d) $\mathbf{e}_\beta$, QIV (sample threshold for QIV: $r_{\text{th}}=0.35$).

significant, ω, ω', $\mathbf{e}_\alpha$, and $\mathbf{e}_\beta$ will occur primarily in the S^+-plane which corresponds to a reverse ''S''-shaped curve in the $\sin(\theta_{\text{pitch}})-\theta_{\text{yaw}}$ plot [Fig. 9(c)].

In the above scenario, it is assumed that ω lies in the S^+-plane and $\mathbf{e}_\gamma$ remains stationary. However, the presence of ω' in other directions (isotropic initial conditions) will vary the rotation of the principal axes. Recall that the distribution for $\mathbf{e}_\gamma$ in the total flow [Fig. 7(c)] follows the S^--plane curve with those of $\mathbf{e}_\beta$ extending outward in this direction as shown in Fig. 7(b). This indicates the occurrence of rotation of $\mathbf{e}_\gamma$ and $\mathbf{e}_\beta$ about the axis of $\mathbf{e}_\alpha$, i.e.,

$$\dot{\Omega}_{\mathbf{e}_\beta-\mathbf{e}_\gamma}=-\frac{1}{\beta-\gamma}\left(\underbrace{\frac{1}{4}\omega_\beta\omega_\gamma}+\tilde{\Pi}_{\beta,\gamma}\right), \tag{3.8}$$

which is induced locally by misaligned vorticity, $\omega_\beta\omega_\gamma$. In this case, Eq. (2.4) indicates that the sense of rotation is such that $\mathbf{e}_\gamma$ is directed *towards* ω. For the assumed conditions, this would result in $|\theta_{\text{yaw}}|<90°$ for $\mathbf{e}_\gamma$. We expect the significance of Eq. (3.8) to be less since ω_γ weakens under vortex contraction. In general, the simultaneous reorientation of the three principal axes given by $\dot{\Omega}$ may result in rather complex trajectories and lead to large variations in orientations.

The spatial orientations of the eigenvectors in the total flow [Figs. 7(a)–7(c)] are consistent with the described dynamics. The shape of the distributions indicate the occurrence of Eq. (3.7) in the S^+-plane and (3.8) in the S^--plane; the former prevailing. The locations of the peaks in $\mathbf{e}_\alpha$ and $\mathbf{e}_\gamma$ are also consistent with the directions of the corresponding axes rotation. In the case of $\mathbf{e}_\beta$, since both Eqs. (3.7) and (3.8) are occurring, more complex distributions of its orientation are expected. Since the rates of locally induced rotation are proportional to the vorticity components, these effects may be particularly significant in QII regions. Recall that in QII, the prevailing orientation of total vorticity ω is $|\theta_{\text{yaw}}|<90°$ [Figs. 5(a) and 5(b)] while that of the fluctuating component ω' is $|\theta_{\text{yaw}}|>90°$ [Fig. 6(a)] which are consistent with the described dynamics [Fig. 9(b)]. The eigenvector orientations [Figs. 7(d)–7(f)] are also consistent. However, re-

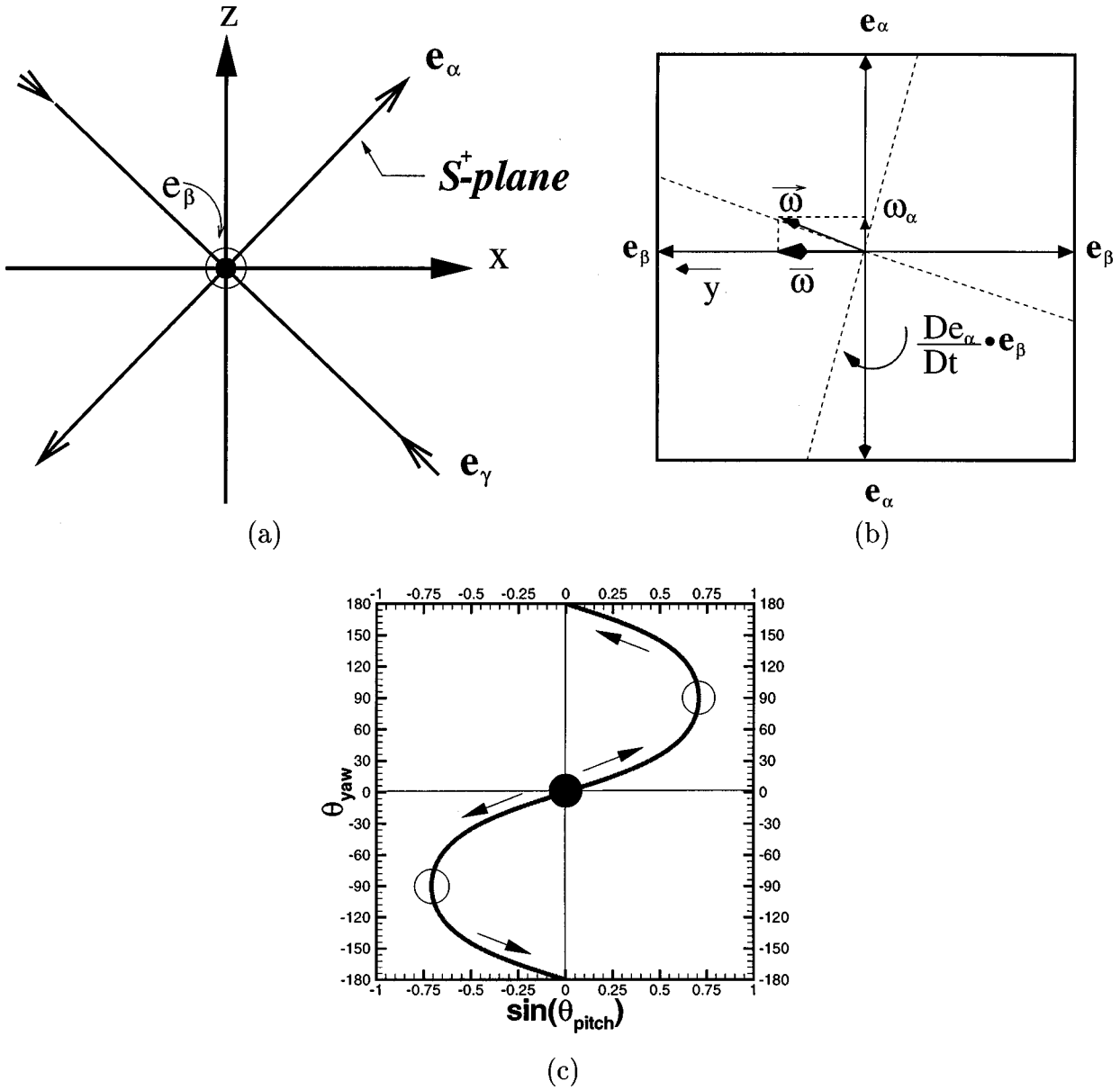

FIG. 9. S-plane structure and dynamics; (a) coordinate system with principal strain eigenvector directions corresponding to mean shear, (b) diagram of S^+-plane indicating locally induced rotation (clockwise) of the principal axes, (c) S^+-plane curve on $\sin(\theta_{\text{pitch}})$ vs θ_{yaw} plot. Note ''○'' indicates orientation of $\bar{\mathbf{e}}_\alpha$, '●' indicates orientation of $\bar{\mathbf{e}}_\beta$, and arrows indicate trajectories of principal axes. Upper right quadrant associated with the *clockwise* rotation of the principal axes as indicated in (b) while lower left quadrant associated with a *counterclockwise* rotation occurring in S^+-plane.

sults for Q0 and QIV (Fig. 8) also show evidence of S-plane dynamics. In high strain regions, strain generation is significant and acts to promote positive β which will then tend to approach α.[1] This will effectively enhance the induced rotation through the prefactor in Eq. (3.7), i.e., $1/(\alpha-\beta)$, thereby retaining its significance in Q0 and QIV regions. In Q0, the S^+-plane curve shape in the distribution of $\mathbf{e}_\alpha$ appears particularly evident [Fig. 8(a)]. In QIV [Figs. 8(c) and 8(d)], the predominant orientations of $\mathbf{e}_\alpha$ and $\mathbf{e}_\beta$ are switched from that of the mean flow.

The directional preferences observed in RHIGH are also exhibited by the RLOW1 flow. The results are quite similar at early times when the values of $r_\omega(t)$ are comparable and relatively high. We note in RHIGH, $r_\omega(t)=10$ at St=9 while in RLOW1, $r_\omega(t)=9$ at St=2. Figure 10 shows JPDs for $\mathbf{e}_\alpha$ and $\mathbf{e}_\beta$ at a later time in RLOW1 (St=6, $r_\omega(t)=7$). The JPDs generally remain similar to those at earlier time although some differences are noted. In QII and Q0, the distributions show less variation and there is greater distinction between the two samples. In particular, the extent of rotation of $\mathbf{e}_\alpha$ and $\mathbf{e}_\beta$ in QII is observed to be greater. From the Q0 results, we see that $\mathbf{e}_\beta$ exhibits a preference for $\theta_{\text{yaw}}\sim 0°$. In the case of QIV, at earlier times (not shown), the distributions of $\mathbf{e}_\alpha$ and $\mathbf{e}_\beta$ are similar to that in the RHIGH flow [Figs. 8(c) and 8(d)], and we note $\mathbf{e}_\alpha$ tends to orient nearly in the spanwise (0°,0°) direction. At St=6 [Figs. 10(c) and 10(f)], the JPDs indicate a reorientation of the axes. These results suggest that QIV regions may be particularly sensitive to flow conditions as characterized by r_ω.

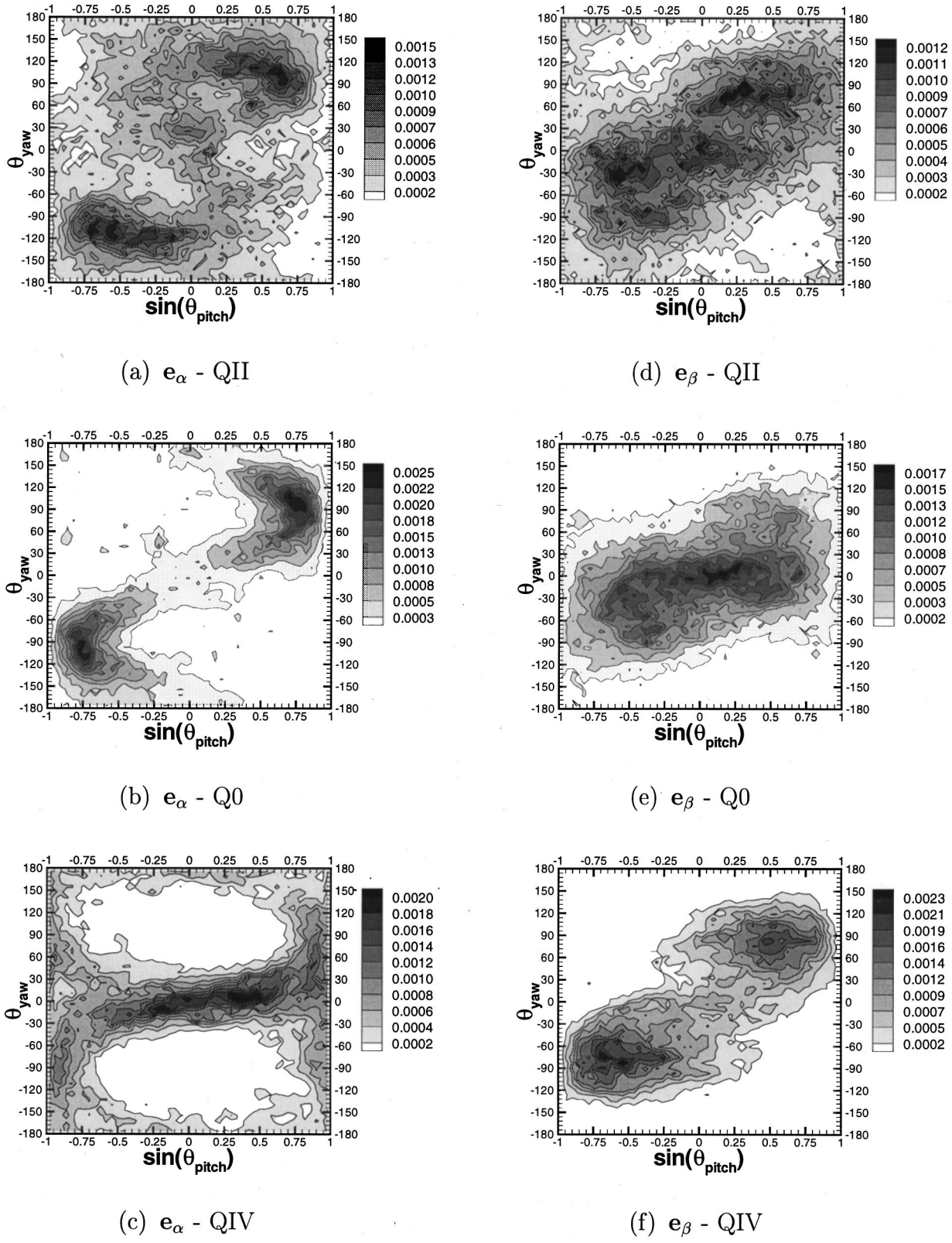

(a) $\mathbf{e}_\alpha$ - QII (d) $\mathbf{e}_\beta$ - QII

(b) $\mathbf{e}_\alpha$ - Q0 (e) $\mathbf{e}_\beta$ - Q0

(c) $\mathbf{e}_\alpha$ - QIV (f) $\mathbf{e}_\beta$ - QIV

FIG. 10. Joint probability distributions indicating the angles of orientation ($\theta_{\text{pitch}}, \theta_{\text{yaw}}$) of eigenvectors $\mathbf{e}_\alpha$ and $\mathbf{e}_\beta$ for QII, Q0, and QIV conditional samples at St=6 (RLOW1): (a)–(c) $\mathbf{e}_\alpha$, (d)–(f) $\mathbf{e}_\beta$ (sample thresholds are QII: $r_{\text{th}}=0.35$, Q0: $r_{\text{th}}=1.3$, QIV: $r_{\text{th}}=0.30$).

Since the described S-plane dynamics result from the influence of the imposed ω and S, we expect that these features will be more prominent in low r_ω flows. Recall in the RLOW2 flow, Re_{λ_0} is comparable to that of RLOW1, however, $r_{\omega_0}=1.8$. Thus, ω' is comparable to S. Since the (nondimensional) time scale associated with the fluctuating vorticity should be of order $S/\omega'=1/r_\omega$, the development of the S-plane dynamics will be more readily observed in this

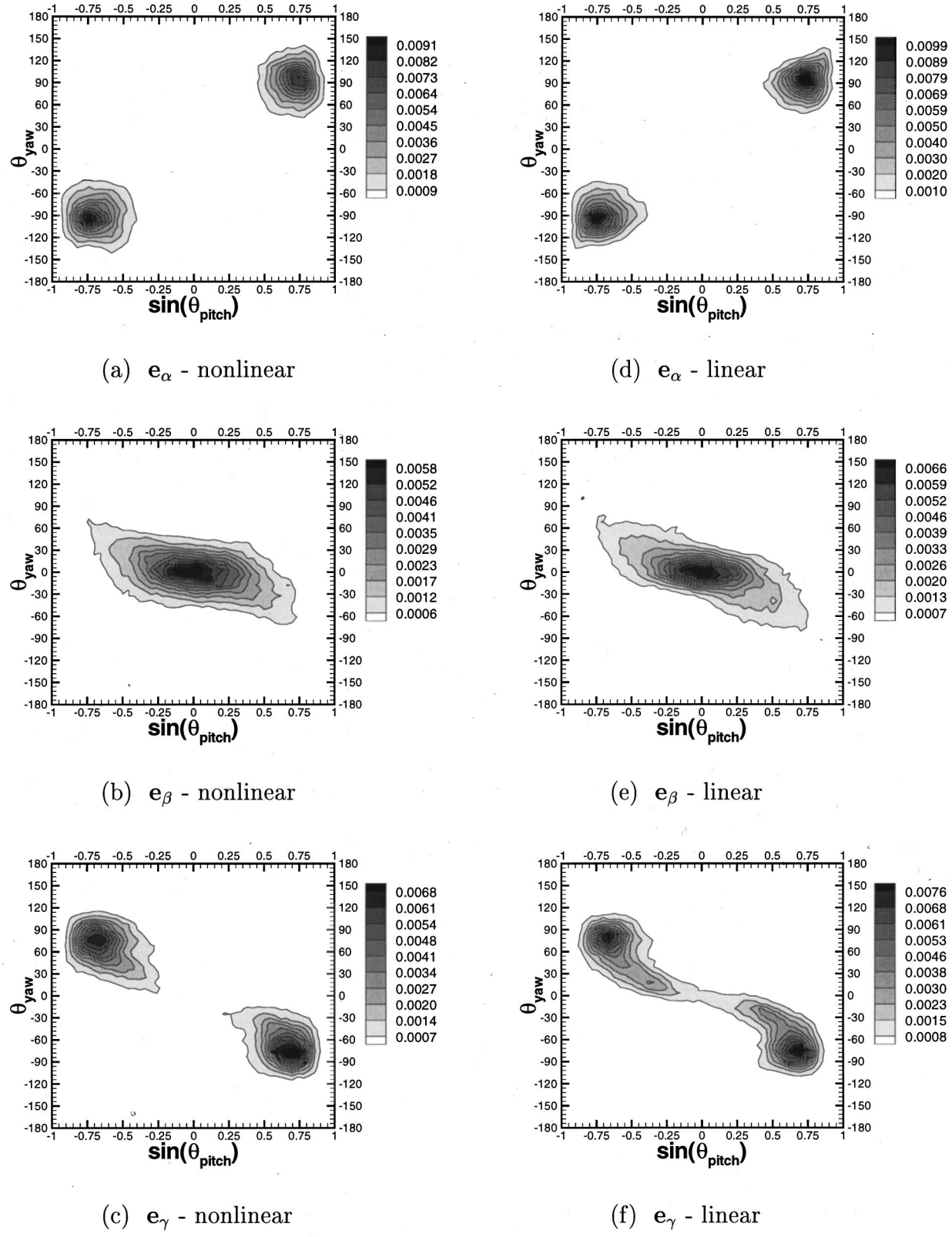

FIG. 11. Joint probability distributions indicating the angles of orientation ($\theta_{\text{pitch}}, \theta_{\text{yaw}}$) of $\mathbf{e}_\alpha$, $\mathbf{e}_\beta$, and $\mathbf{e}_\gamma$ for QII sample: (a)–(c) nonlinear ($r_{\text{th}}=0.25$), (d)–(f) linear ($r_{\text{th}}=0.20$) results (RLOW2 simulation—St=1.0).

flow. To further investigate the dynamics and help distinguish nonlinear effects, a simulation of the linearized Navier–Stokes equations using the same inital flow field as RLOW2 was also performed.

At early times, characteristics of the nonlinear and linear RLOW2 flows are similar. Figure 11 shows results for St=1 for QII. We see from the distributions of $\mathbf{e}_\beta$ and $\mathbf{e}_\gamma$ the occurrence of Eq. (3.8), i.e., S^--plane dynamics. In these

flows, $\overline{\omega}$ is significant ($r_\omega \sim 1$) and since QII consists of high ω^2, this sampling initially favors ω' oriented towards the positive y axis (since $\overline{\omega}$ is in this direction). This implies that $\omega_\alpha \ll \omega_\beta \approx \overline{\omega}$ and thus, the *extent of rotation* in the S^+-plane, i.e., rotation of $\mathbf{e}_\beta$ towards ω and $\mathbf{e}_\alpha$ away from ω, will be small. This results in a *shorter* trajectory along the S^+-plane curve as indicated by the JPDs of $\mathbf{e}_\alpha$ [Figs. 11(a) and 11(d)] in which the peaks correspond to θ_{yaw} only slightly beyond $\pm 90°$. Since the sense of rotation in the S^--plane is such that $\mathbf{e}_\gamma$ rotates towards ω [Eq. (2.4)], the extent of rotation in this plane will be larger, i.e., $\mathbf{e}_\gamma$ must rotate further to align with ω. This corresponds to a *longer* trajectory along the S^--plane curve which is clearly evidenced in Figs. 11(e) and 11(f). These results indicate the significance of local geometry and the association with r_ω.

At later times, the nonlinear and linear flows generally differ although some similarities are maintained. Figure 12 shows the orientation of $\mathbf{e}_\alpha$ for each of the conditional samples at St=6. In comparing the nonlinear RLOW2 results [Figs. 12(a)–12(c)] with those of RLOW1 [Figs. 10(a)–10(c)], we see that in the case of QII and Q0, the corresponding results show the same basic features. In QII, $\mathbf{e}_\alpha$ [Fig. 12(a)] exhibits $|\theta_{\text{yaw}}| > 90°$ while tending towards lower θ_{pitch} values. In the case of the linear flow [Fig. 12(d)], there is significantly less variation in the orientation of $\mathbf{e}_\alpha$ and higher θ_{pitch} is maintained. In Q0 [Fig. 12(b)], $\mathbf{e}_\alpha$ exhibits ''C''-shaped distributions about the location of $\overline{\mathbf{e}}_\alpha$. The similarity of the linear flow [Fig. 12(e)] indicates that Q0 regions are dominated by linear effects. The corresponding orientations of $\mathbf{e}_\beta$ and $\mathbf{e}_\gamma$ in the linear flow are shown in Fig. 13. As indicated in Fig. 13(a), the orientation of $\mathbf{e}_\beta$ exhibits a preference for $\theta_{\text{yaw}} \sim 0°$ with a range of θ_{pitch}, i.e., $\mathbf{e}_\beta$ tends to orient in the $y-z$ plane. From Fig. 13(b), we see that $\mathbf{e}_\gamma$ tends to exhibit ''C''-shaped distributions about $\overline{\mathbf{e}}_\gamma$. These basic features are also exhibited in the nonlinear RLOW2 flow (not shown). The simultaneous rotation of $\mathbf{e}_\alpha$ and $\mathbf{e}_\gamma$ may explain the observed behavior of $\mathbf{e}_\beta$. In QIV regions of the nonlinear flow [Fig. 12(c)], the distributions tend to differ from those in RLOW1 and RHIGH with $\mathbf{e}_\alpha$ orienting more closely to $\overline{\mathbf{e}}_\alpha$. In the linear case [Fig. 12(f)], a similar tendency for $\mathbf{e}_\alpha$ to reorient is exhibited although the spanwise direction appears to be conspicuously avoided.

Thus far, we have considered only local effects. We now consider the *net* rate of rotation $\dot{\Omega}_{\mathbf{e}_\alpha - \mathbf{e}_\beta}$ [Eq. (3.7)] which includes the effects of $\tilde{\Pi}$. Probability distributions of $\dot{\Omega}_{\mathbf{e}_\alpha - \mathbf{e}_\beta}$ and the separate components indicate that negative values of $\dot{\Omega}_{\mathbf{e}_\alpha - \mathbf{e}_\beta}$ correspond to the dominance of locally induced rotation $(-\omega_\alpha \omega_\beta / 4(\alpha - \beta))$ while positive values correspond to the dominance and positivity of nonlocally induced rotation $(-\tilde{\Pi}_{\alpha\beta}/(\alpha - \beta))$. In general, locally induced rotation tends to dominate. The expected value $\langle \dot{\Omega}_{\mathbf{e}_\alpha - \mathbf{e}_\beta} \rangle_{\mathbf{e}_\alpha}$, conditioned on the orientation of $\mathbf{e}_\alpha$, was also evaluated (not shown). Distributions of $\langle \dot{\Omega}_{\mathbf{e}_\alpha - \mathbf{e}_\beta} \rangle_{\mathbf{e}_\alpha}$ for a given conditional sample are similar in all three flows and indicate that the most probable orientations of $\mathbf{e}_\alpha$ are generally associated with moderately low rotation rates which will tend to have longer duration. Overall, the most active regions exhibiting the highest magnitudes of $\dot{\Omega}_{\mathbf{e}_\alpha - \mathbf{e}_\beta}$ are those of QII. From the corresponding $\langle \dot{\Omega}_{\mathbf{e}_\alpha - \mathbf{e}_\beta} \rangle_{\mathbf{e}_\alpha}$, we find that as $\mathbf{e}_\alpha$ orients towards the horizontal, reduced rotation rates are observed. Conditional expectation of the nonlocally induced rotation (not shown) shows significant positive values associated with these events which may be acting to redirect $\mathbf{e}_\alpha$. Additional statistics indicate that nonlocally induced rotation is most significant in these regions and, as will be shown, tends to counteract locally induced rotation.

In Q0 regions, $\langle \dot{\Omega}_{\mathbf{e}_\alpha - \mathbf{e}_\beta} \rangle_{\mathbf{e}_\alpha}$ exhibits negative and rather uniform, moderately low magnitudes along the ''C''-shaped distribution in $\mathbf{e}_\alpha$. We now discuss the dynamics of these regions in more detail. Recall that the positive direction (orientation) of $\mathbf{e}_\alpha$ is defined by the projection of ω on the line of action of $\mathbf{e}_\alpha$. In the S^+-plane scenario, initial amplification of ω' is along $\overline{\mathbf{e}}_\alpha$. If $\omega' \gg \overline{\omega}$, the extent of rotation of $\mathbf{e}_\alpha$ (away from ω) will be significant. However, as $\mathbf{e}_\alpha$ reorients along the S^+-plane curve from $(\pm 45°, \pm 90°)$ and towards $(0°, \pm 180°)$, α will contribute to amplification of spanwise ω. If this is significant, ω will become oriented further towards the spanwise direction. However, negative $\dot{\Omega}_{\mathbf{e}_\alpha - \mathbf{e}_\beta}$ will continue to act to redirect $\mathbf{e}_\alpha$ away from ω. The associated trajectory of $\mathbf{e}_\alpha$ is along a segment of the S^+-plane curve corresponding to $|\theta_{\text{yaw}}| < 90°$ with direction towards $(\mp 45°, \mp 90°)$. The probable orientations for $\mathbf{e}_\alpha$ would thus comprise ''C''-shaped curves centered near the $\overline{\mathbf{e}}_\alpha$ positions in the angle pair plot. We expect the described process to be significant in Q0 regions where both ω and S are significant. The processes are linear and thus observed in the linear flow [Fig. 12(e)]. We note that at later times (St>6), the orientation of the S axes associated with this sample do not change significantly suggesting that the described dynamics establish an effective quasi-equilibrium condition.

In the case of QIV regions, although the orientation of $\mathbf{e}_\alpha$ differs between RLOW1 and RLOW2, the distributions of $\langle \dot{\Omega}_{\mathbf{e}_\alpha - \mathbf{e}_\beta} \rangle_{\mathbf{e}_\alpha}$ are found to be similar. We may expect that strain-dominated regions will depend on the relative significance of background ω' and $\overline{\omega}$, i.e., r_ω. In QIV regions of RLOW2, $\overline{\omega}$ remains significant and ω will tend to orient towards the spanwise direction. The extent of rotation in the S^+-plane will not be great and $\mathbf{e}_\alpha$ remains near $\overline{\mathbf{e}}_\alpha$ [Fig. 12(c)]. In the RLOW1 (and RHIGH) flow, the fluctuating fields dominate. Results from RLOW1 at very early times (St$\ll$1) show nearly isotropic orientation in ω and $\mathbf{e}_\alpha$. As the flow develops, ω' is established in the direction of $\overline{\mathbf{e}}_\alpha$ and this is followed by a preferential orientation of $\mathbf{e}_\alpha$ in the spanwise direction. The former observation suggests the significance of persistent straining. Later in time (St=6), ω tends to orient towards the spanwise direction due to amplification of $\overline{\omega}$. We also observe a tendency for redirection of $\mathbf{e}_\alpha$ away from the spanwise direction [Fig. 10(c)] consistent with the associated negative $\langle \dot{\Omega}_{\mathbf{e}_\alpha - \mathbf{e}_\beta} \rangle_{\mathbf{e}_\alpha}$. In the RHIGH flow,

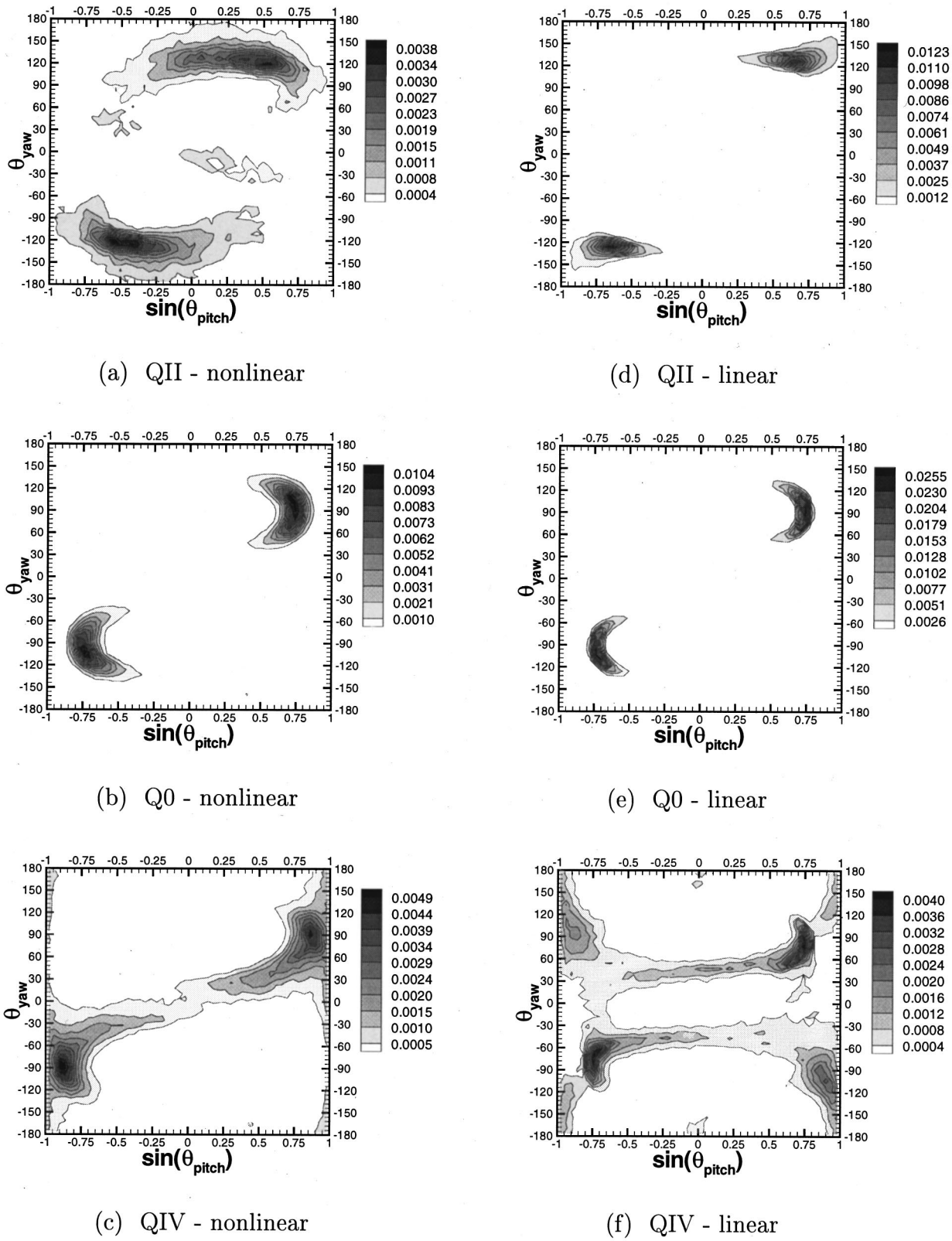

FIG. 12. Joint probability distributions indicating the angles of orientation ($\theta_{\text{pitch}}, \theta_{\text{yaw}}$) of $\mathbf{e}_\alpha$ for QII, Q0, and QIV conditional samples: (a)–(c) nonlinear, (d)–(f) linear results (RLOW2 simulation at St=6.0. Sample thresholds for nonlinear results are QII: $r_{\text{th}}=0.15$, Q0: $r_{\text{th}}=1.3$, QIV: $r_{\text{th}}=0.12$. Thresholds for linear results are QII: $r_{\text{th}}=0.10$, Q0: $r_{\text{th}}=1.3$, QIV: $r_{\text{th}}=0.08$).

the relative significance of ω is much weaker and may explain the higher probability for $\mathbf{e}_\alpha$ to remain in this direction [Fig. 8(c)]. Strain-dominated regions may thereby sustain anisotropy in the flow as r_ω increases.

We now consider characteristics of $\tilde{\Pi}$ in more detail. As discussed earlier, the effects of $\tilde{\Pi}_{\alpha\beta}$ are significant in QII regions of the flow. Figure 14 shows a scatter plot of the locally- and nonlocally induced rotation terms in Eq. (3.7)

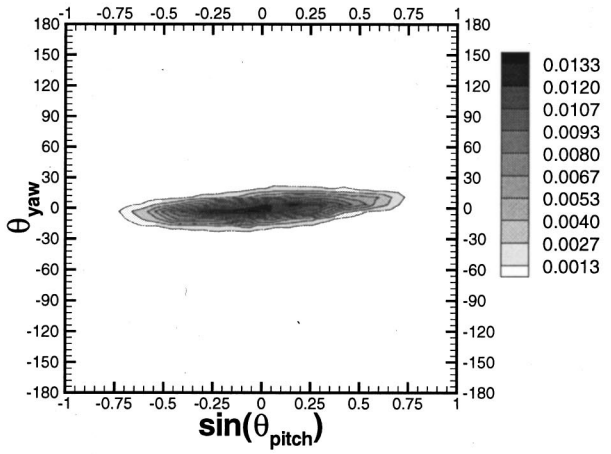

(a) $\mathbf{e}_\beta$

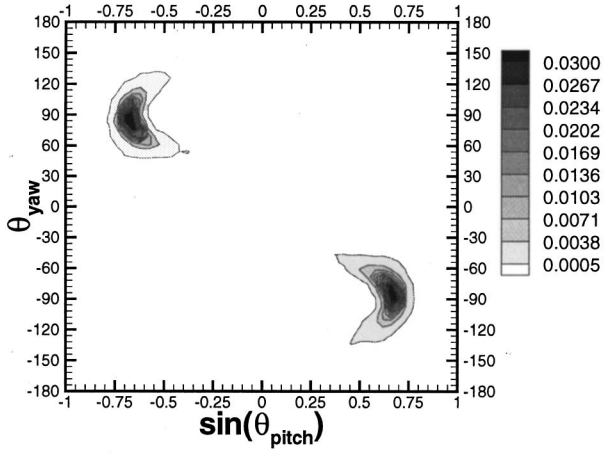

(b) $\mathbf{e}_\gamma$

FIG. 13. Joint probability distributions indicating the angles of orientation ($\theta_{\text{pitch}}, \theta_{\text{yaw}}$) of (a) $\mathbf{e}_\beta$ and (b) $\mathbf{e}_\gamma$ for Q0 conditional sample in linear flow (RLOW2 simulation—St=6.0).

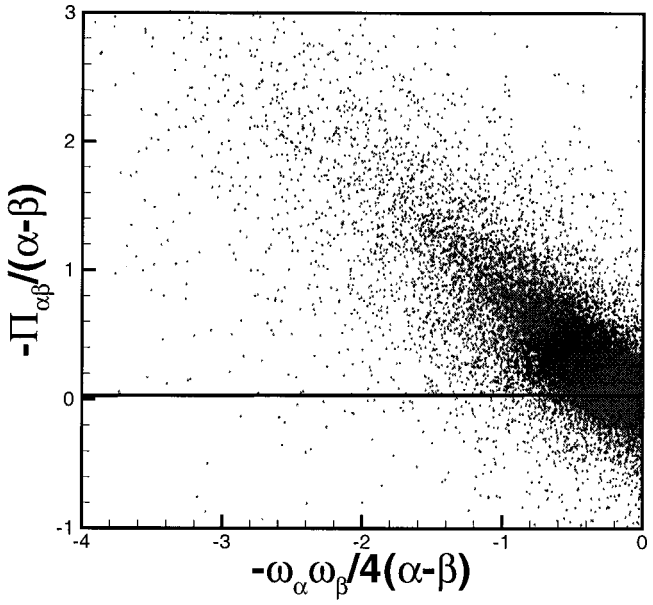

(a) nonlinear flow

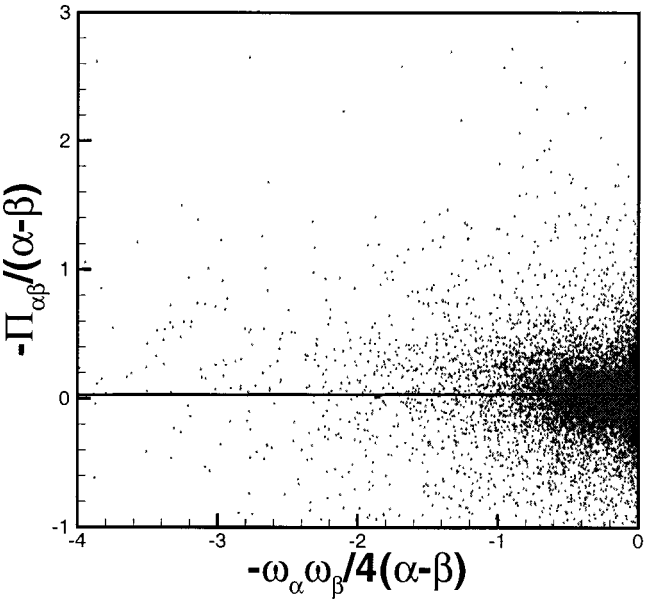

(b) linear flow

FIG. 14. Scatter plots showing correlation between $-\tilde{\Pi}_{\alpha\beta}/(\alpha-\beta)$ and $-\omega_\alpha\omega_\beta/4(\alpha-\beta)$ for QII conditional sample (RLOW2—St=6.0); (a) nonlinear and (b) linearized shear flow. Values are normalized by $\langle\omega^2\rangle^{1/2}$.

for the QII sample in the nonlinear and linear RLOW2 flows. In the nonlinear flow [Fig. 14(a)], the behavior is similar to that in isotropic turbulence[1] and indicates a strong negative correlation, i.e., the nonlocally induced rotation $-\tilde{\Pi}_{\alpha\beta}/(\alpha-\beta)$ tends to *counteract* the locally induced rotation $-\omega_\alpha\omega_\beta/4(\alpha-\beta)$. The same behavior is exhibited in the RHIGH and RLOW1 flows. As indicated by the $\langle\dot{\Omega}_{\mathbf{e}_\alpha-\mathbf{e}_\beta}\rangle_{\mathbf{e}_\alpha}$ results, the implication is to effectively impede the rotation of the strain axes by redirecting $\mathbf{e}_\alpha$. In QII of the linear flow [Fig. 14(b)], values of $-\tilde{\Pi}_{\alpha\beta}/(\alpha-\beta)$ are reduced considerably. In the case of Q0 (not shown), the behavior of the nonlinear and linear flows are quite similar. In QIV (also not shown), $-\tilde{\Pi}_{\alpha\beta}/(\alpha-\beta)$ tends to become uncorrelated with $-\omega_\alpha\omega_\beta/4(\alpha-\beta)$, particularly in the higher r_ω flows.

As discussed in Nomura and Post,[1] the correlation between $-\omega_\alpha\omega_\beta/4(\alpha-\beta)$ and $-\tilde{\Pi}_{\alpha\beta}/(\alpha-\beta)$ exhibited by QII events in isotropic turbulence is associated with the strong tendency for ω to align with the eigenvector $\mathbf{f_3}$ corresponding to the smallest eigenvalue of Π, ϕ_3, in rotation-dominated regions. Figure 15 shows the conditional expectation of $\cos\theta$ conditioned on the value of II (for $III<0$) indicating the relative orientation of ω with each of the eigenvectors of S and Π (here, θ is the angle between ω and eigenvector). The nonlinear flow [Fig. 15(a)] again exhibits behavior similar to isotropic turbulence;[1] that is, an increasing tendency for ω to align with $\mathbf{f_3}$ with increasing (positive) II. This tendency is much stronger than that associated with the alignment of ω with $\mathbf{e}_\beta$. In the case of the linear flow [Fig. 15(b)], the tendency for alignment of ω with $\mathbf{f_3}$ is not exhibited at high positive II. In fact, there are no strong

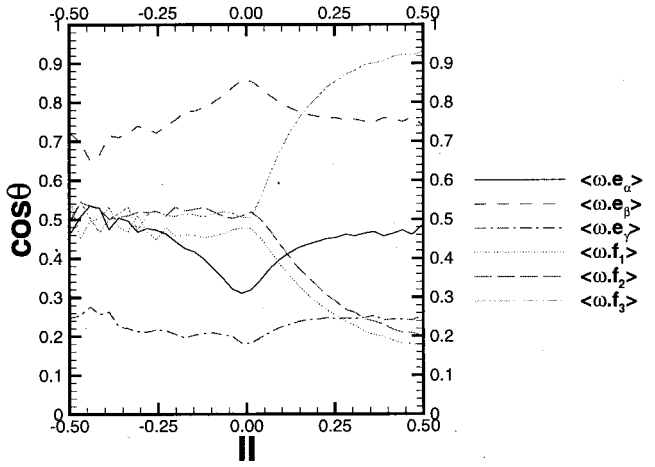

(a) nonlinear flow

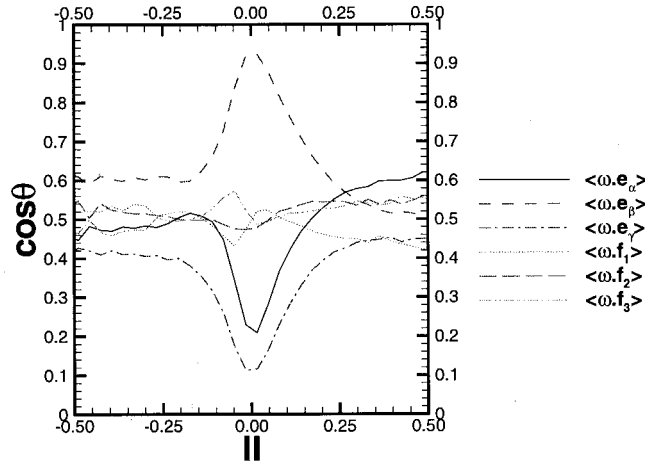

(b) linear flow

FIG. 15. Conditional expectation of $\cos\theta$ indicating relative orientation between ω and each of the eigenvectors of S and Π (conditioned on the value of II with $III<0$) for (a) nonlinear and (b) linearized shear flow (RLOW2—St=6.0).

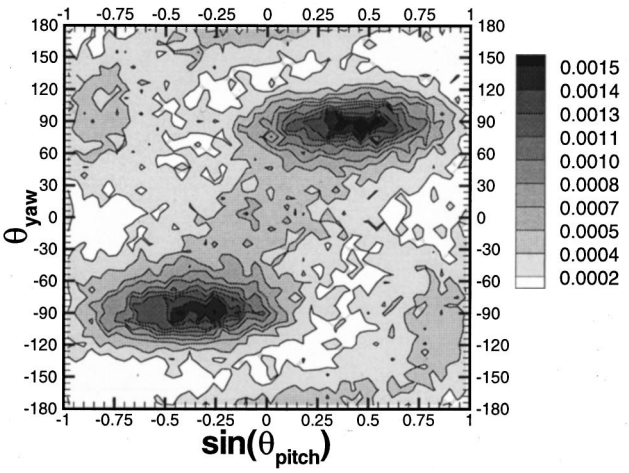

(a) $St = 3$

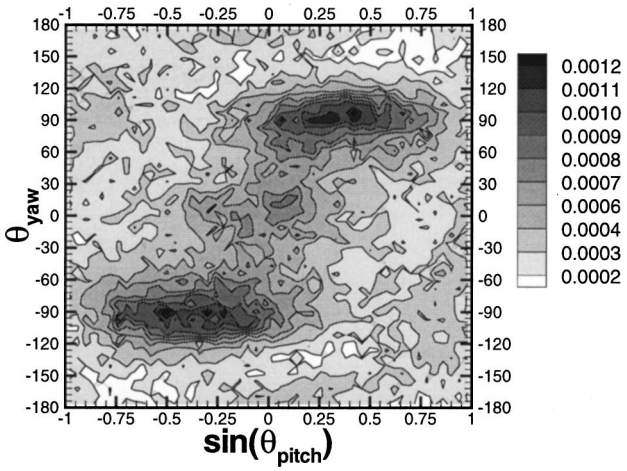

(b) $St = 9$

FIG. 16. Joint probability distributions indicating the angles of orientation ($\theta_{\text{pitch}}, \theta_{\text{yaw}}$) of Π eigenvector, $\mathbf{f_3}$, for QII sample (RHIGH): (a) St=3, (b) St=9.

tendencies for any alignment in these regions. The preferential alignment that occurs is that of ω and $\mathbf{e}_\beta$ which develops in regions associated with $II \approx 0$ which include Q0 events. This is, of course, an attribute of the uniform shear flow.

Probability distributions of the eigenvalues of Π in QII for the fully nonlinear shear flow (not shown) indicate ϕ_3 values nearly zero while the other two eigenvalues are positive. The physical implication of the alignment of ω with $\mathbf{f_3}$, where $\phi_3 \sim 0$, in high $II>0$ regions is the presence of cylindrical spatial structure as indicated by the Burgers vortex tube.[1] As observed in Fig. 3, $II>0$ regions do exhibit similar geometric structure. The spatial orientation of $\mathbf{f_3}$ in QII regions of RHIGH is shown in Fig. 16. The location of the peaks are near those of ω [Figs. 5(a) and 5(b)]. However, there is a subtle difference in the shape of the distributions. As the flow develops, the peaks of $\mathbf{f_3}$ *maintain* $\theta_{\text{yaw}} = \pm 90°$ indicating a strong streamwise component. It is expected that mean advection will incline these structures towards the streamwise direction.[9] This may explain the observed behavior of $\mathbf{f_3}$ which is associated with the pressure field. As suggested by Fig. 12(a) and the $\langle \dot{\Omega}_{\mathbf{e}_\alpha - \mathbf{e}_\beta} \rangle_{\mathbf{e}_\alpha}$ results, the induced rotation of the S axes through $\tilde{\Pi}$ tends to redirect, e.g., $\mathbf{e}_\alpha$ away from the S^+-plane course. The absence of these effects in the linear flow is indicated in Fig. 12(d) which shows $\mathbf{e}_\alpha$ maintaining higher values of θ_{pitch}.

Characteristics of Π are thus influenced by the proximate spatial structure. The implications of Π on the dynamics are established in the strain basis [Eqs. (2.1)–(2.2)]. Probability distributions of the normalized strain basis components $\tilde{\Pi}_{ij}$ for the QII sample in the nonlinear and linear flows are shown in Fig. 17. The behavior of the nonlinear flow is again similar as that of isotropic turbulence[1] while the linear flow exhibits distributions which are nearly symmetric about zero. In QII regions of the nonlinear flow [Fig. 17(a)], the diagonal components dominate and all three exhibit predominantly positive values (recall $\text{tr}[\Pi] = 2II = \omega^2/2 - \mathsf{S}^2$). The magnitudes of the off-diagonal components of $\tilde{\Pi}$ are

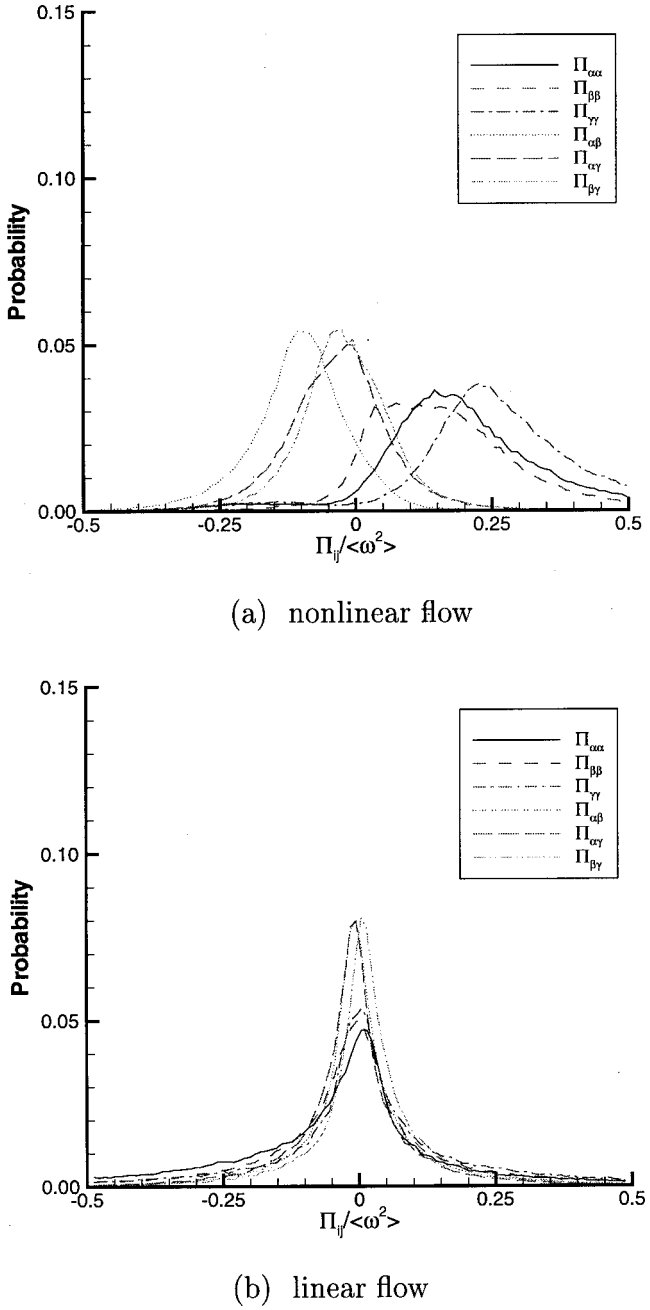

FIG. 17. Probability distributions of the strain basis components $\tilde{\Pi}_{ij}$ (normalized by $\langle\omega^2\rangle$) for QII conditional sample: (a) nonlinear and (b) linearized shear flow (RLOW2—St=6.0).

generally smaller and $\tilde{\Pi}_{\alpha\beta}$ is the dominant component with its peak occurring at a negative value. In QII regions of the linear flow [Fig. 17(b)], $\tilde{\Pi}$ appears to be nearly isotropic (note in the linearized equations, $\mathrm{tr}[\Pi] \neq \omega^2/2 - \mathsf{S}^2$). Visualization of high amplitude rotation-dominated isosurfaces in the linear flow (not shown) show elongated structures that incline from the streamwise x direction with $\theta_{\mathrm{pitch}} < 45°$ and $\theta_{\mathrm{yaw}} \sim 90°$. However, based on the characteristics of Π, these structures are not consistent with vortex tubes. It is likely that these isosurfaces represent regions of concentrated ω^2 reorganized by mean advection rather than what are considered to be *coherent* structures. In the case of Q0 (not shown), the distributions of $\tilde{\Pi}$ for the nonlinear and linear flow are similar consistent with the dominance of linear effects in these regions. In QIV (also not shown), although the linear flow exhibits a more symmetric distribution, the diagonal components remain somewhat negatively skewed.

Figure 18 shows the joint probability of the $II-III$ invariants for the nonlinear and linear RLOW2 flows. The nonlinear flow [Fig. 18(a)] is similar to those of RLOW1 and RHIGH (Fig. 2) although the distribution is more confined for $II>0$. This may be associated with the greater significance of the imposed mean strain as suggested by the Burgers vortex model.[1] In the linear flow [Fig. 18(b)], the preference for the upper left (QII) quadrant is not as strong and the distribution of points in the upper half plane ($II>0$) is more symmetric. As indicated by Eq. (2.2), local ω generates positive strain in the orthogonal plane. In the nonlinear flow, initial amplification of ω_α will promote positive β. In the linear flow, early time amplification of ω_α will not directly promote β since this is a nonlinear effect. Probability distributions of the principal eigenvalues for QII in the linear flow (not shown) indicate a development towards symmetric distributions with the peak in β approaching zero. This is consistent with the more vertical distribution of points observed in the upper half $II-III$ plane (Fig. 18) and suggests development towards a locally two-dimensional state in rotation-dominated regions. In the nonlinear flow, a positive skewness in the distribution of β is maintained indicating active vortex stretching and associated energy transfer. In regard to strain-dominated regions, the preference for the lower right (QIV) quadrant observed in the nonlinear flows is maintained by the linear flow. This may be due to the effects of $\tilde{\Pi}$ which tend to be retained in these regions.

IV. CONCLUSIONS

This paper describes the structure and dynamics associated with the interaction of vorticity ω and rate-of-strain S in homogeneous sheared turbulence. In particular, characteristics of S and the pressure Hessian Π, which previously have not been considered, are presented. The coupled dynamics of ω and S are effectively described in the principal strain basis[1] which distinguishes vortex stretching and rotation of the principal axes of S. The latter mechanism includes both local and nonlocal effects and is associated with misaligned ω with respect to the principal axes. Nonlocal effects act through the anisotropic part of Π. To investigate the dynamics in detail, conditional sampling based on the invariants of the velocity gradient tensor is employed. This differentiates structure and assists in distinguishing various mechanisms by considering the relative significance of rotation versus strain. In general, the high amplitude conditional samples capture the basic features observed in the total flow. Comparison of the results with those of isotropic turbulence establish generality of the described dynamics; the underlying behavior of ω and S is found to be similar in these flows. In the case of shear, the physical implications of the associated mechanisms and, in particular, the relevance of local geometry are revealed.

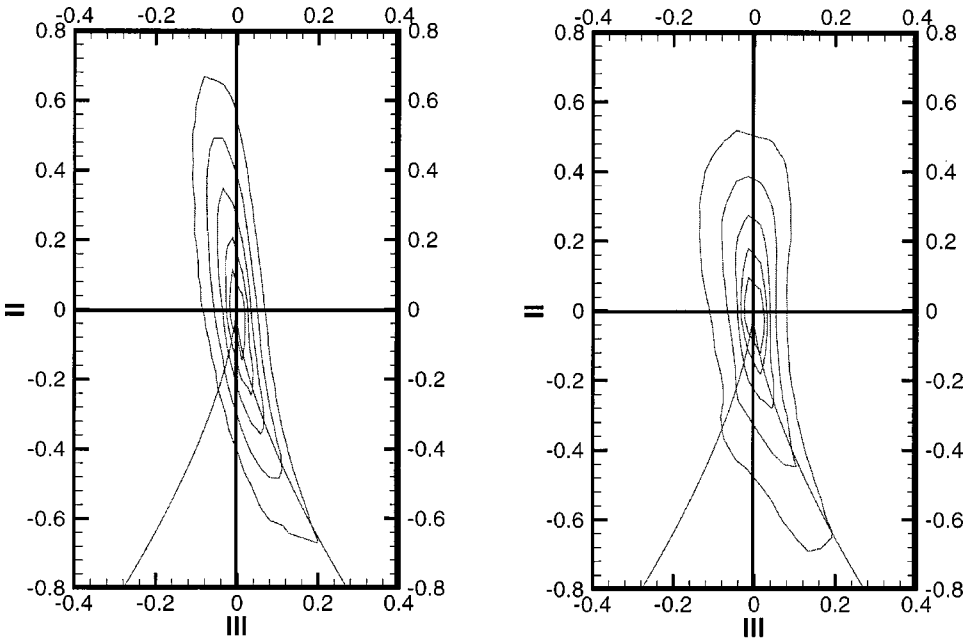

FIG. 18. Joint probability distribution of the tensor invariants II and III (normalized by $\langle\omega^2\rangle$ and $\langle\omega^2\rangle^{3/2}$, respectively) for nonlinear and linear flows (RLOW2—St=6.0). Contour values correspond to $\log(10^6 P+1)$ where P is the probability. The minimum and maximum contour levels are 2.0 and 4.5, respectively, where the latter corresponds to the inner most contour.

Due to the imposed mean shear, the spatial orientation of ω and the principal axes of S exhibit distinct directional preferences. Initial stretching of fluctuating ω by mean extensional strain and the presence of mean vorticity establish a *predominant* misalignment of ω with respect to the principal axes of S. This results in locally induced rotation of the principal axes which establishes preferential orientation in S thereby directing further development of ω'. As in isotropic turbulence, high amplitude rotation-dominated regions are characterized by tube-like spatial structure as indicated by the strong alignment of ω with the eigenvector of Π corresponding to its smallest (nearly zero) eigenvalue. This produces a counteracting nonlocally induced rotation of the principal axes which thereby affects the orientation of S in these regions. In the presence of mean shear, the eigenvectors of Π in these regions also exhibit directional preference which may include the influence of mean advection. In regions with significant S, the behavior of the principal strains effectively enhances the rate of rotation of the strain axes so that it remains important. In regions where both ω and S are significant, reorientation of the S axes will contribute to amplification of spanwise ω which, in turn, will affect the relative orientation of ω. The S axes tend to equilibrate in these regions as a result of this feedback. These primarily linear effects result in a predominance of spanwise and vertical ω. In high amplitude strain-dominated regions, the orientation of the S axes is particularly sensitive to $r_\omega=\omega'/S$ since the extent of rotation of the axes is dependent on local geometry which is associated with the relative significance of $\overline{\omega}$.

Simulation results of the linearized Navier–Stokes equations exhibit similar early time local dynamics. However, they lack the distinct nonlocal features present in the nonlinear flow. In particular, characteristics of Π differ significantly. The strain basis components exhibit nearly symmetric distributions about zero. This suggests the absence of nonlocal effects as represented by the restricted Euler equations in which isotropic Π acts to preserve the volume of a fluid element with no directional distinction. In high amplitude rotation-dominated regions in fully nonlinear flow, Π exhibits distinct directionality with respect to ω due to the presence of spatial structure. In the corresponding regions of the linear flow, such directionality does not exist. This indicates that the (nonlinear) influence of the surrounding flow is absent, i.e., there is no spatial *coherence*.

In general, the characteristics of Π are similar in both isotropic and homogeneous sheared turbulence and is consistent with similar small-scale structure. Although the structures tend to exhibit preferential spatial orientation in the shear flow, this does not appear to affect measures in the strain basis, e.g., the *relative* orientation of small-scale quantities. We expect that the effects associated with the mean flow will be weaker in flows with high $r_\omega\sim \mathrm{Re}_\lambda/\mathrm{Sh}$. The shorter timescales result in considerable variation in spatial orientation of the principal axes. In particular, rotation-dominated regions are controlled by fluctuating ω and thus tend to exhibit increasing variation as the flow develops. However, as the present results show, preferential orientation of the S axes, particularly in strain-dominated regions, is maintained in the high r_ω flow. It is, therefore, not clear that directional features will be eliminated with high r_ω. The *continual* presence of the mean vorticity and strain may be a significant factor in the dynamics despite their relatively weak magnitudes.

ACKNOWLEDGMENTS

We gratefully acknowledge Frank Jacobitz and Sutanu Sarkar for use of their DNS database. We also appreciate the helpful comments provided by the Referees of our manuscript. In particular, we thank one of the Referees for point-

ing out the bias in θ_{pitch}. The authors are indebted to the University of California, San Diego for support for this research. The first author also gratefully acknowledges support through the Hellman Fellows Program.

[1]K. K. Nomura and G. K. Post, ''The structure and dynamics of vorticity and rate of strain in incompressible homogeneous turbulence,'' J. Fluid Mech. **377**, 65 (1998).
[2]P. Vieillefosse, ''Internal motion of a small element of fluid in an inviscid flow,'' Physica A **125**, 150 (1984).
[3]Z.-S. She, E. Jackson, and S. A. Orszag, ''Structure and dynamics of homogeneous turbulence: models and simulations,'' Proc. R. Soc. London, Ser. A **434**, 101 (1991).
[4]J. Jimenez, A. A. Wray, P. G. Saffman, and R. S. Rogallo, ''The structure of intense vorticity in isotropic turbulence,'' J. Fluid Mech. **255**, 65 (1993).
[5]R. M. Kerr, ''Higher-order derivative correlations and the alignment of small-scale structures in isotropic numerical turbulence,'' J. Fluid Mech. **153**, 31 (1985).
[6]W. T. Ashurst, A. R. Kerstein, R. M. Kerr, and C. B. Gibson, ''Alignment of vorticity and scalar gradient with strain rate in simulated Navier–Stokes turbulence,'' Phys. Fluids **30**, 2343 (1987).
[7]K. K. Nomura and S. E. Elghobashi, ''Mixing characteristics of an inhomogeneous scalar in isotropic and homogeneous sheared turbulence,'' Phys. Fluids A **4**, 606 (1992).
[8]M. Tanaka and S. Kida, ''Characterization of vortex tubes and sheets,'' Phys. Fluids A **5**, 2079 (1993).
[9]S. Kida and M. Tanaka, ''Dynamics of vortical structures in a homogeneous shear flow,'' J. Fluid Mech. **274**, 49 (1994).
[10]M. M. Rogers and P. Moin, ''The structure of the vorticity field in homogeneous turbulent flows,'' J. Fluid Mech. **176**, 33 (1987).
[11]T. Gerz, J. Howell, and L. Mahrt, ''Vortex structures and microfronts,'' Phys. Fluids **6**, 1242 (1994).
[12]J. C. H. Fung, ''Shear flow turbulence structure and its Lagrangian statistics,'' Fluid Dyn. Res. **17**, 147 (1996).
[13]P. J. Diamessis and K. K. Nomura, ''The interaction of vorticity, rate-of-strain, and scalar gradient in stratified homogeneous sheared turbulence,'' to appear in Phys. Fluids (2000).
[14]B. J. Cantwell, ''Exact solution of a restricted Euler equation for the velocity gradient tensor,'' Phys. Fluids A **4**, 782 (1992).
[15]T. Gerz, U. Schumann, and S. Elghobashi, ''Direct simulation of stably stratified homogeneous turbulent shear flows,'' J. Fluid Mech. **200**, 563 (1989).
[16]F. Jacobitz, S. Sarkar, and C. Van Atta, ''Direct numerical simulations of the turbulence evolution in a uniformly sheared and stably stratified flow,'' J. Fluid Mech. **342**, 231 (1997).
[17]F. Jacobitz, ''Direct numerical simulation of turbulent stratified shear flowm'' Ph.D. Dissertation, University of California, San Diego (1998).
[18]B. J. Cantwell, ''On the behavior of velocity gradient tensor invariants in direct numerical simulations of turbulence,'' Phys. Fluids A **5**, 2008 (1993).